Response to co-editor comments on:

"Evaluation of biomass burning aerosols in the HadGEM3 climate model with observations from the SAMBBA field campaign"

Thank you for your helpful comments.

We agree that there is considerable variability in the OC:OA ratio in observations and that the current ratio of 1.4 in GLOMAP-mode is at the very minimum of the observed range. Increasing this would have an important bearing on the global emission scaling factors and so this is an important point to bring out more strongly in the manuscript.

From reviewing the literature estimates of OA:OC range from 1.4 to 3.2 for organic aerosol mixtures, but with a clear trend towards increasing OA:OC with more aged aerosol mixtures. This makes it is difficult to determine an upper bound for POM:OC in the freshly emitted particles. In section 2.3.2 we'd concluded:

"*Recent analyses of aerosol mass spectra (e.g. Aitken et al., 2008; Ng et al., 2010; Tiitta et al., 2014; Brito et al., 2014) and preliminary analysis of airborne data from SAMBBA indicate POM:OC ratios in the range 1.5 – 1.8 for fresh particles / near-source emissions. However, the observations indicate considerable variability with aerosol age and source region with POM:OC ratios increasing to 2.0-2.3 for aged and more highly oxidised aerosol. This introduces considerable uncertainty in gauging a representative POM:OC for global models where near-source ageing may not be represented."*

There is also some uncertainty for global models on whether a value representative of freshly emitted particles is relevant or a value representing "young" aerosol after some near-source ageing. This depends on whether there is a representation for near-source ageing in the model (there is not yet for GLOMAP-mode). Therefore, there is certainly scope to increase OC:POM in GLOMAP-mode and decrease the global emission scaling factor. As an example, the global emission scaling factor for GLOMAP-mode could be reduced to 1.5 if the POM:OC ratio was increased to 1.9, which would still be a credible value for BB emissions. Doing this would reduce the BC:OA ratio and perhaps require revisions to BC refractive index or OC refractive index (brown carbon) to compensate.

Please find the revised manuscript with tracked changes in red and comments to explain how the change addresses the comments. The text in the manuscript has

been altered in the following three sections to bring out these points:

(i) Abstract

(ii) Section 2.3.1 (Global emission scaling factor

(iii) Section 4 (Conclusions)

Evaluation of biomass burning aerosols in the HadGEM3 climate model with observations from the SAMBBA field campaign

B. T. Johnson[1], J. M. Haywood[1,2], J. M. Langridge[1], E. Darbyshire[3], W. T. Morgan[3], K. Szpek[1], J. Brooke[1], F. Marenco[1], H. Coe[3], P. Artaxo[4], K. M. Longo[5*], J. Mulcahy[1], G. Mann[6], M. Dalvi[1], and N. Bellouin[7]

[1]Met Office, Exeter, UK

[2]CEMPS, University of Exeter, Exeter, UK

[3]Centre for Atmospheric Science, University of Manchester, Manchester, UK

[4]Physics Institute, University of São Paulo, São Paulo, Brazil

[5]National Institute for Space Research (INPE), São José dos Campos, Brazil

*Now at NASA Goddard Space Flight Center and USRA/GESTAR, Greenbelt, MD, USA

[6]National Centre for Atmospheric Science, School of Earth and Environment, University of Leeds, Leeds, UK

[7]Department of Meteorology, University of Reading, Reading, UK

Correspondence email: ben.johnson@metoffice.gov.uk

Abstract

We present observations of biomass burning aerosol from the South American Biomass Burning Analysis (SAMBBA) and other measurement campaigns, and use these to evaluate the representation of biomass burning aerosol properties and processes in a state-of-the-art climate model. The evaluation includes detailed comparisons with aircraft and ground data, along with remote sensing observations from MODIS and AERONET. We demonstrate several improvements to aerosol properties following the implementation of the GLOMAP-mode modal aerosol scheme in the HadGEM3 climate model. This predicts the particle size distribution, composition and optical properties, giving increased accuracy in the representation of aerosol properties and physical-chemical processes over the CLASSIC bulk aerosol scheme previously used in HadGEM2. Although both models give similar regional distributions of carbonaceous aerosol mass and Aerosol Optical Depth (AOD), GLOMAP-mode is better able to capture the observed size distribution, single scattering albedo, and Ångström exponent across different tropical biomass burning source regions. Both aerosol schemes overestimate the uptake of water compared to recent observations, CLASSIC more so than GLOMAP-mode, leading to a likely overestimation of aerosol scattering, AOD and single scattering albedo at high relative humidity. Observed aerosol vertical distributions were well captured when biomass burning aerosol emissions were injected uniformly from the surface to 3 km. Finally, good agreement between observed and modelled AOD was gained only after scaling up GFED3 emissions by a factor of 1.6 for CLASSIC and 2.0 for GLOMAP-mode. We attribute this difference in scaling factor mainly to different assumptions for the water uptake and growth of aerosol mass during ageing via oxidation and condensation of organics. We also note that similar agreement with observed AOD could have achieved with lower scaling factors if the ratio of organic carbon to primary organic matter was increased in the models toward the upper range of observed values. Improved knowledge from measurements is required to reduced uncertainties in emission ratios for black carbon and organic carbon, and the ratio of organic carbon to primary organic matter for primary emissions from biomass burning.

Comment [b1]: As suggested by the co-editor we bring out the issue with OC:POM ratio and emission ratios in the abstract.

1 Introduction

Biomass burning is a major source of tropospheric aerosol globally (van der Werf et al., 2010) and dominates the aerosol burden in many tropical regions. Carbonaceous aerosols are

produced from open burning of vegetation, including both wild fires and managed fires for clearing forest, pasture and arable land. These aerosols have a wide range of impacts (Voulgarakis and Field, 2015) including short-term influences on local and regional weather (e.g. Kolusu et al., 2015) and significant impacts on regional air quality and human health (Johnston et al., 2012; Reddington et al. 2015). They also have a significant role in climate change as they affect the global energy budget in a number of ways (e.g. IPCC, 2013; Bauer and Menon 2012, Haywood and Boucher 2000).

The aerosols emitted from biomass burning (BB) are composed primarily of organic carbon and black carbon and they both scatter and absorb solar radiation in the atmosphere. Such aerosol-radiation interactions lead to large reductions of surface insolation and significant radiative heating of the atmosphere (Ramanathan and Carmichael, 2008; Johnson et al., 2008a; Malavelle et al., 2011; Milton et al., 2008). These effects may suppress the hydrological cycle by stabilizing the lower troposphere, although strong absorption can in some cases enhance precipitation regionally by increasing low-level convergence (Wu et al., 2013; Ramanathan et al., 2001; Lau et al., (2006); Randles et al., 2008). The enhancement of particulate numbers by BB can also increase the concentration of cloud condensation nuclei modifying cloud microphysical properties (Spracklen et al., 2011). This can brighten clouds (Twomey 1974) and modelling studies have also shown that smoke (aerosol) from BB can delay the onset of precipitation and influence the evolution of convective clouds (Andreae et al., 2004; Feingold et al. 2001). The localised heating associated with absorption of solar radiation by the emitted particles can also suppress convection and change regional cloud cover via the semi-direct aerosol effect (Koren et al., 2008; Tosca et al., 2014).

Quantifying the impact of BB aerosol emissions on the global radiation budget and climate is therefore difficult with many competing effects and sources of uncertainty (Ten Hoeve et al., 2012; Ward et al. 2012). Recent assessments suggest that on a global basis, changes in the top of the atmosphere (TOA) radiation budget resulting from increased scattering due to aerosol emitted from BB is approximately cancelled by increased absorption by the aerosol (Myhre et al., 2013; Shindell et al., 2013; Bellouin et al., 2013). However, the extent to which scattering and absorption compensate varies regionally as it depends on many factors including the surface albedo, cloud cover, and the Lauoptical properties of the aerosol. In particular, the single scattering albedo (e.g. Myhre et al., 2008), and the vertical distribution of the absorbing aerosol relative to clouds (e.g. Samset et al., 2013) have a strong influence on this potential

balance. Absorption depends mainly on the black carbon content of the aerosol, but a significant contribution in the UV, and to a lesser extent visible spectrum, can come from organics, i.e. brown-carbon (Saleh et al., 2014).

Overall, BB aerosol emissions are estimated to lead to a global mean negative Effective Radiative Forcing (ERF) as aerosol-cloud interactions in models are shown to exert a negative forcing that outweighs any small positive forcing from aerosol-radiation interactions. This is expected to have a cooling influence on global climate but the ERF and global temperature responses are estimated to be relatively small, compared to those from sulphates or black carbon from fossil fuel combustion (Jones et al., 2007; Shindell et al., 2013). Nevertheless, increases in aerosol due to BB have potentially important impacts on regional climates, via changes in atmospheric circulation and shifts in precipitation (Tosca et al., 2010, 2013; Ott et al., 2010; Zhang et al., 2009; Jones et al., 2007).

Recent studies have also highlighted more complex Earth-system interactions associated with BB emissions. By scattering solar radiation and increasing the ratio of diffuse to direct radiation at the surface, aerosol can enhance photosynthesis over tropical forests, increasing Net Primary Productivity (NPP) and carbon uptake (Rap et al., 2015; Mercado et al. 2009). On the other hand, tropospheric ozone produced due to NOx emissions from fires can damage plants, reducing NPP (Pacifico et al. 2015). Mao et al. (2013) also showed that emission of aerosol and trace gases from BB led to increases in global tropospheric ozone and methane lifetime. In their study this led to a positive radiative forcing that offset the negative radiative forcing from the sum of aerosol-radiation and aerosol-cloud interaction effects.

Quantifying these wide-ranging impacts of BB on climate, air quality and the earth-system relies on the accurate representation of BB processes and aerosol properties in global models. It is therefore important to evaluate their simulation in models with observations to reduce inherent biases and identify priorities for future improvements to emissions, processes and techniques used to represent aerosol properties. The properties of aerosols in BB-dominated air masses have been investigated during a number of field experiments (e.g. Kaufmann et al., 1998; Swap et al., 2002; Haywood et al., 2008), and reviewed by Reid et al. (2005a, 2005b) and Martin et al. (2010). A new set of observations is now available from the South American Biomass Burning Analysis (SAMBBA), a field campaign that took place in Brazil during 14 September – 4 October 2012. The measurement campaign was a joint UK-Brazil project led by the Met Office and NERC, in collaboration with the National Institute of Space Studies in

Brazil (INPE) and University of Sao Paulo (USP) in Brazil. The campaign involved the UK Facility for Airborne Atmospheric Measurements (FAAM) BAe-146 atmospheric research aircraft coordinated with a range of ground-based observations (Allan et al., 2014; Brito et al., 2014; Marenco et al., 2016). The airborne campaign comprised 20 flights investigating aerosol properties, atmospheric chemistry, clouds, meteorology and the radiation budget over Amazonia. The flights provided intensive measurement of aerosols across Amazonia including aerosol dominated by BB emissions.

In this study we combined the observations from SAMBBA with those from previous campaigns and from long-term remote sensing observations (MODIS, AERONET) to evaluate the representation of Biomass Burning Aerosol (BBA) in a state-of-the-art global climate model, the Hadley Centre Global Environment Model version 3 (HadGEM3). We evaluate two aerosol schemes: (i) the mass-based CLASSIC aerosol scheme, (ii) the microphysical scheme GLOMAP-mode. CLASSIC was previously used in HadGEM2-ES for CMIP5 (Bellouin et al., 2011) and in this study is used within HadGEM3. GLOMAP-mode has been implemented more recently in the Met Office Unified Model and is available in HadGEM3 (e.g. Bellouin et al., 2013) (in some publications configurations of HadGEM3 that include GLOMAP-mode have been referred to as HadGEM-UKCA). The study focuses on aerosol properties important in simulating aerosol-radiation interactions, including the global distribution of aerosol and their physical, chemical and optical properties. The study provides an assessment of the influence of biomass burning on aerosol properties, as simulated by each scheme, and assesses some of the assumptions commonly used to represent BB aerosol emissions and aerosol processes in global models.

2 Methods

2.1 HadGEM3 model configuration

This work uses global simulations of the Met Office Unified Model (MetUM) within the framework HadGEM3 (Hewitt et al., 2011). The scientific configuration of the physical model was from the Global Atmosphere 7 (GA7) configuration and our simulations ran with a resolution of N96 (1.25˚ x 1.875˚) and 85 vertical levels. Sea surface temperatures and sea ice were prescribed using reanalysed daily-varying fields for the period 2002 – 2011 based on the methodology of Reynolds et al. (2007) (as used in Atmosphere Model Intercomparison

Project). The atmospheric circulation was free-running including aerosol-radiative effects from either CLASSIC or GLOMAP-mode. The atmospheric physics configuration includes some updates to atmospheric processes over previous configurations presented in Williams et al. (2015) and Walters et al. (2014). The main update affecting this study is the implementation of the Global Model for Aerosol Processes (GLOMAP-mode) (Mann et al., 2010) modal aerosol scheme. The implementation of GLOMAP-mode in the MetUM took place as part of the UKCA (United Kingdom Chemistry and Aerosol) project along with several alternative atmospheric chemistry schemes. In this study we use an offline-chemistry configuration where concentrations of gas phase chemical species [ozone (O_3), hydrogen peroxide (H_2O_2), and the hydroxyl (OH), nitrate (NO_3) and hydroperoxyl (HO_2) radicals] required for the oxidation of aerosol precursor species are provided as monthly mean climatologies. The climatology of oxidants was generated from a previous 20-year simulation that included on-line gas-phase atmospheric chemistry using the UKCA combined tropospheric and stratospheric chemistry scheme (O'Connor et al., 2014; Morgenstern et al., 2009). For this study a parallel simulation was also run with the same model configuration except that aerosols were simulated by the CLASSIC (Coupled Large-scale Aerosol Scheme for Simulations in Climate Models) aerosol scheme. CLASSIC was the aerosol scheme used in HadGEM2, including Hadley Centre contributions to the fifth Coupled Model Intercomparison Project (CMIP5) (Bellouin et al., 2011). CLASSIC used a climatology of oxidants generated separately from an earlier simulation. For both aerosol schemes fire emissions of BBA were taken from the Global Fire Emission dataset (GFED) version 3.1 (van der Werf et al., 2010). We use monthly mean emissions averaged over the period 2002 – 2011. Details of how these were implemented are given in section 2.3. Anthropogenic emissions of SO_2 and carbonaceous aerosol (from fossil fuel and bio-fuel) for both aerosol schemes were based on the 10-year average emissions from 2002-2011. These data were provided by MACC/CityZEN (via ECCAD-Ether at http://eccad.sedoo.fr) that interpolates across this time frame using historical emissions for 2000 from ACCMIP (Lamarque et al., 2010) and emissions for 2005 and 2010 from the RCP8.5 scenario (Granier et al. 2011; Diehl et al., 2012). However, we keep annual emissions constant at the 2002 – 2011 mean rate. Volcanic degassing emissions of SO_2 were taken from Andres and Kasgnoc (1998). Emissions of di-methyl sulphide (DMS) were calculated from the Kettle et al. (1999) ocean DMS climatology with the Liss and Merlivat (1986) surface-exchange parameterization.

Stratospheric aerosol was represented via the climatology from Cusack et al. (1998). Nitrate aerosols were not included in this study.

2.2 Representation of aerosols

2.2.1 CLASSIC

CLASSIC is a mass-based or "bulk" aerosol scheme that represents a range of aerosol species (sulphate, fossil-fuel soot, fossil-fuel organic carbon, BBA, sea salt, and mineral dust) as separate externally-mixed species with specified physical and optical properties. A full description of the scheme is available in the appendix of Bellouin et al. (2011). CLASSIC includes a representation of the sulphur cycle for the gas-phase and aqueous-phase production of sulphate aerosol. Carbonaceous aerosols are represented as three separate species depending on their emission source (soot, fossil-fuel organic carbon, BBA). Each has different assumptions regarding their physical, chemical and optical properties. The representation of the BBA species is based on the aircraft observations of Haywood et al. (2003) and Abel et al. (2003) obtained over Southern Africa during SAFARI-2000 and is described in more detail below. Mineral dust is simulated by the 6-bin scheme of Woodward (2001), with modifications in Woodward (2011). CLASSIC uses a diagnostic scheme for wind-driven sea salt, i.e. sea salt aerosol is not transported but instead is diagnosed locally over ocean points as a function of wind speed and with a prescribed scale-height in the vertical (see Bellouin et al., 2011, Jones et al., 2001). Secondary Organic Aerosol (SOA) is not modelled explicitly by CLASSIC but the contribution to AOD and radiative effects is included using an offline climatology. The SOA climatology is provided by the UK Met Office Chemistry Transport Model (STOCHEM) (Derwent et al. 2003) based on the emission of isoprene from biogenic sources.

The BBA species includes a fresh mode to represent the primary particles, and an aged mode to represent the aerosols after chemical ageing and growth. A third tracer is used to track the mass of in-cloud BBA particles that are either lost via wet deposition or return to the aged BBA mode as rain water is lost via evaporation. The size distribution for each mode is represented by a single log-normal with a standard deviation of 1.3 and mean diameter of 0.2 μm for the fresh mode and 0.24 μm for the aged mode. The total aerosol mass emitted into the fresh mode is taken as the sum of BC and OC from GFED but the model makes its own assumptions regarding the proportion of BC and OC in each BBA mode. Each BBA mode is

assumed to be an internal mixture of Black Carbon (BC) and Organic Carbon (OC) with an organic carbon mass fraction of 91.5 % for the fresh mode and 94.6 % for the aged and in-cloud modes. The ageing process occurs on a 6-hour e-folding timescale and during the transfer from the fresh to aged mode the aerosol mass is increased by a factor of 1.62. This representation of aerosol ageing is based on the evolution of aerosol properties in a large smoke plume observed during SAFARI-2000 (Abel et al., 2003). Optical properties are calculated from Mie theory with the refractive index (RI) computed as the volume-weighted average of the BC and OC components assuming an aerosol mass density of 1.35g/cm^3 for the OC and 1.7g/cm^3 for the BC. The RI of the BC component is based on WCP (1983) (1.75 – 0.44i at 550nm) and the RI of the OC component is assumed to be 1.53 – 0.0i across the solar spectrum. This gives an RI of 1.54 - 0.025i for the fresh mode and 1.54 – 0.018i for the aged mode, in the mid-visible (550nm). Both species are hygroscopic with empirical growth curves from Magi and Hobbs (2003) (Section 3.5).

2.2.2 GLOMAP-mode

The GLOMAP-mode (Global Model for Aerosol Processes) scheme (Mann et al., 2010) has an entirely different modelling philosophy to CLASSIC, being an aerosol microphysics scheme including a size-resolved representation of the key processes which alter the particle physical and chemical properties during its lifecycle (e.g. Mann et al., 2014). The configuration of GLOMAP-mode in this study (GA7) includes four soluble modes (nucleation, Aitken, accumulation, coarse) and one insoluble Aitken mode, and includes the components of sulphate, particulate organic matter, black carbon and sea salt. Aerosol particles within any given mode are assumed to be an internal mixture of the chemical constituents in that mode. Particles within a mode can grow by condensation and coagulation. Aerosol mass and number can also be transferred from smaller to larger modes, either via coagulation between the modes, or as the diameter of particles within a mode exceeds the specified limit for that mode (Mann et al., 2010). Insoluble Aitken particles also age as sulphuric acid and oxidised organic vapours condense onto them and the aerosol are transferred to the Aitken soluble mode when the coating exceeds 10 mono-layers. Although GLOMAP-mode generally treats mineral dust within the modal framework, in the same way as other aerosol components, in the runs here, this modal representation for mineral dust was not used. Instead, for the GA7 configuration of the atmospheric model applied here,. the existing UM bin-resolved dust scheme (Woodward, 2001; Woodward et al., 2011) was used

to transport dust (and apply its radiative effects) alongside the GLOMAP representation for other components (as in Bellouin et al., 2013). The simulation with GLOMAP-mode included primary aerosol emissions from biomass burning, bio-fuel and fossil fuel combustion sources, interactive sea spray emissions, and sub-grid sulphate particle formation (so-called "primary sulphate"), assumed to be 2.5 % of emitted SO_2. The scheme explicitly represents the secondary aerosol particle source from binary nucleation of sulphuric acid vapour and water vapour applying the parameterization of Kulmala et al. (1998). The transfer of secondary organic aerosol (SOA) mass to the particle phase occurs following the oxidation of emitted biogenic Volatile Organic Compounds (bVOCs), chemically producing a zero vapour pressure gas phase species "SEC_ORG" which then condenses on to existing particles (increasing the OA mass in each mode). In these simulations, no anthropogenic SOA was produced, and the only SOA-producing bVOC being a lumped monoterpene species "MONOTER" produced by emissions from Guenther et al., (1995). The chemical production of SEC_ORG from MONOTER proceeds via reaction with OH, NO_3 and O_3, with rates given by oxidation rates for alpha-pinene, and assuming a 26 % molar yield to the particle phase. The 26% value increased from the 13% used by Bellouin et al. (2013) to account for missing SOA from isoprene.

Aerosol particle emissions from biomass burning are assumed to have an initial (emitted) size distribution given by a single log-normal mode with geometric mean diameter of 0.15 µm and geometric standard deviation of 1.59, as used by Stier et al. (2005) and consistent with the range of log-normal parameters fitted to BB aerosol size distributions in Fig. C2 of Dentener et al. (2006). The ratio of BC to OC varies interactively in GLOMAP-mode depending on mixing of these components from the range of sources mentioned above. There is currently no representation of the SOA from semi-volatile VOCs partitioning into the aerosol particle phase.. In GLOMAP-mode, the BC component of carbonaceous particles is always assumed hydrophobic, whereas the POM component is assumed to be hydrophobic in insoluble particles, and hydrophilic in soluble particles. Further details on the hygroscopic growth are given in section 3.5. Aerosol optical properties are derived for each mode as function on aerosol mode diameter and RI using look-up-tables with pre-computed results from Mie theory. For these the RI is computed by volume-weighted averages depending on the mixture of components within any given mode. The RI of the BC component, as in CLASSIC, is based on WCP (1983) and the OC component is assumed to be non-absorbing with an RI of

1.5 – 0.0i across the solar spectrum. Aerosol mass density for BC and OC are both assumed to be 1.5 g/cm^3.

2.3 Biomass burning aerosol emissions and scaling factors

2.3.1 Global emission scaling factor

Fire emissions of BBA were taken from the Global Fire Emission Dataset (GFED) version 3.1 (van der Werf et al., 2010). Preliminary simulations with GFED3.1 emissions led to large underestimates in modelled aerosol mass and AOD over tropical BB regions. Therefore, we apply global scaling factors of 1.6 for CLASSIC and 2.0 for GLOMAP-mode (Table 1) to increase the total BB aerosol emissions to give better agreement between modelled and observed mid-visible AOD (see section 3.1). These scaling factors were not calculated precisely but were found to give good overall correspondence between modelled and observed peak AODs (from AERONET and MODIS) over continental BB source regions in the tropics, and a consistent AOD contribution from BB emissions in CLASSIC and GLOMAP-mode over the BB source regions. Other modelling studies have also found it necessary to apply global scaling factors to increase aerosol emissions from BB sources to gain realistic AOD and/or particulate mass concentrations (Kaiser et al., 2012; Marlier et al., 2013; Petrenko et al., 2012; Tosca et al., 2013; Archer-Nicholls et al., 2016; Kolusu et al., 2015; Reddington et al., 2016). Note, observed AODs are also used to derive biome-specific or spatially varying scaling factors in some top-down emission estimation methods such as the Quick Fire Emission Dataset QFED (Darmenov and da Silva 2013) and the Fire Energetics and Emissions Research (FEER) (Ichoku and Elison 2014) and these lead to global total particulate matter emissions approximately 2-3 times greater than GFED3.1 (Ichoku and Elison 2014). However, we acknowledge that the discrepancy between modelled and observed AOD (prior to emission scaling) could be due to other biases or missing processes in the models.

In the CLASSIC simulation the global scaling factor of 1.6 (Table 1) was applied to the total mass emitted into the BBA tracer. For GLOMAP-mode a factor of 2.0 was applied to the BB emissions of aerosol mass (both the OC and BC component) and number. The scaling used here differs between the two aerosol schemes, and the aim of doing so is to quantify the magnitude of the discrepancy between modelled and observed AOD (prior to scaling), and

highlight the fact that the discrepancy depends on assumptions and processes internal to the aerosol schemes themselves. It should be noted that the scaling factors found here could be substantial reduced the overall mass of carbonaceous aerosol was increased in the models. This could have been achieved either by increasing the ratio of organic carbon to primary organic matter (section 2.3.2 below), or in the case of GLOMAP-mode by including a representation for secondary organic aerosol formation from VOCs emitted during BB (section 2.3.3).

Comment [b2]: As suggested by the co-editor we are careful to explain that the OC:POM ratio could have been increased and this would substantially alter the global tuning factors required.

2.3.2 Scaling of organic carbon to primary organic matter

In this study biomass burning emissions of the organic aerosol component are derived from the OC flux provided by GFED3.1. As OC represents the mass of the carbon only, the contribution of other elements (principally oxygen) to the total organic aerosol mass (i.e. Primary Organic Matter POM) must be considered separately. In CLASSIC no scaling is applied to convert the mass of OC to POM. In GLOMAP-mode OC is converted to POM assuming a POM:OC mass ratio of 1.4 (Table 1). This conversion factor of 1.4 has been broadly used in atmospheric models and was originally based on analysis of filter measurements of fresh urban emissions from the 1970's onwards (see Turpin and Lim, 2001 and references therein). More recent analyses of aerosol mass spectra (e.g. Aitken et al., 2008; Ng et al., 2010; Tiitta et al., 2014; Brito et al., 2014) and preliminary analysis of airborne data from SAMBBA indicate POM:OC ratios in the range 1.5 – 1.8 for fresh particles / near-source emissions from biomass burning. Therefore, an upward adjustment from the 1.4 conversion factor widely assumed may be warranted to more accurately simulate the aerosol mass emissions from BB. However, the observations indicate considerable variability with aerosol age and source region with POM:OC ratios increasing to 2.0-2.3 for aged and more highly oxidised aerosol. This introduces considerable uncertainty in gauging a representative POM:OC for global models where near-source ageing may not be represented.

2.3.3 Growth of organic aerosol component during ageing

In CLASSIC the condensation of VOCs onto BBA is represented in a simplified manner increasing the aerosol mass by a factor of 1.62 (Table 1) when the fresh BB mode is converted to the aged mode. This scaling factor is based on measurements from a large plume during SAFARI-2000 (Abel et al. 2003). However, the evidence for growth of aerosol mass in BB plumes is mixed. For example, Vakkari et al. (2014) concluded that oxidation and

subsequent secondary aerosol formation were important in the evolution of smoke plumes 2-4 hours after emission. In contrast, other studies based on aircraft measurements of aerosol composition and emission ratios have shown no net mass gain, or even net loss of aerosol mass between fresh and aged plumes, despite oxidation (chemical aging). These studies include measurements from West Africa (Capes et al. 2008), from SAMBBA (Morgan et al. 2012), and from a synthesis of the West African measurements with three other campaigns (Jolleys et al., 2012). These suggest that evaporation of organic material after initial emission outweighs or at least compensates for mass added due to secondary formation of organic aerosol. The assumed growth in CLASSIC is therefore not fully supported by recent observational analyses and is an aspect of the scheme that must be considered as we evaluate the model.

The configuration of GLOMAP-mode here does not include secondary aerosol formation from VOCs emitted by biomass burning, or the associated variation of POM:OC during chemical ageing. This is acknowledged as a potentially large source of bias that may to some extent necessitate the global emission scaling.

2.3.4 Vertical injection height assumptions

Smoke plumes can rise several kilometres before detraining into the atmosphere, although this depends critically on fire size / heat flux and atmospheric stability (Freitas et al., 2007). Regional assessments show that the majority of smoke plumes detrain in the boundary layer with maximum plume heights typically below 2 km, whereas vigorous plumes from some large fires can extend into the free troposphere up to altitudes 6 km or more in exceptional cases (Freitas et al., 2007; Kahn et al., 2008; Val Martin et al., 2010; Val Martin et al., 2012; Sofiev et al., 2012; Tosca et al., 2011). During SAMBBA the concentration of aerosol was generally highest in the lowest 2 – 3 km (corresponding to the maximum height of the atmospheric boundary layer) and declined rapidly with height above this (Marenco et al., 2015). Tenuous aerosol layers were frequently observed in the mid-troposphere up to altitudes of 5 or 6 km but given the prevalence moist convection during SAMBBA (mainly in the Western region) it was difficult to determine whether these elevated layers related to plume injection heights or were the result of vertical transport and detrainment from cumulus (in some cases pyrocumulus were also observed).

HadGEM3 does not include an explicit smoke plume-rise model but prescribes the vertical profile of emissions depending on vegetation type provided by GFED. Following

recommendations from the 1st phase of AeroCom (see section 7 and Fig. 9 of Dentener et al., 2006) fire emissions from peat fires, savannah and woodland are assumed to have small plume rise and are emitted at the lowest model level, allowing sub-grid scale turbulence to mix these through the boundary layer. Emissions from forest and tropical deforestation fires are assumed to have more significant plume rise and are injected uniformly from the surface to an assumed maximum injection height of 3 km. These injection height assumptions were used identically for both the CLASSIC and the GLOMAP-mode simulations to maintain consistency.

2.4 Experimental design of simulations

Five simulations were completed, each with a 3 month spin up followed by a 10 year run with emissions, SSTs and sea ice based on the years 2002-2011. The main two simulations that are evaluated in this study are: (i) CLASSIC aerosols with BB emission scaling factor of 1.6, (ii) GLOMAP-mode aerosols with BB emission scaling factor of 2.0. A third simulation with GLOMAP-mode with no BB aerosol emissions was required to enable the contribution of BB emissions to AOD and aerosol mass to be inferred. Furthermore, to illustrate why emission scaling was necessary we also include results in section 3.1 from CLASSIC and GLOMAP-mode simulations without scaling of BB emissions. Apart from these changes in the simulation of aerosols the scientific configuration of the atmospheric model was identical in all simulations. In these simulations the atmospheric circulation was free-running (not nudged to meteorological analyses) and so a ten year period is required to average over interannual variability of meteorology. The selected time period 2002 – 2011 spans the last 10 years where GFED3.1 data was available. One advantage of selecting this time period rather than earlier years is that the GFED3.1 emissions benefit from inclusion of the burned area product from Aqua MODIS from 2002 onwards. Unfortunately, the GFED3.1 data were not available for 2012 (the period of the SAMBBA campaign). For this reason the evaluations against aircraft campaign data in this study focus on the intrinsic properties of BBA (physical, chemical and optical properties) that are expected to depend more on the vegetation and burning practices in the observed regions than on year-to-year variability of burned area.

2.5 In situ observations from SAMBBA and other biomass burning campaigns

Aircraft measurements of aerosol properties have been taken from the SAMBBA campaign that took place in Brazil during Sept-Oct 2012. As the aerosol properties differed regionally

we present average properties separately for the Western region (flights based from Rondonia: 7-12.5°S, 58-65°W) and Eastern region (flights over Tocantins: 10-12°S, 46.5-49°W) (Fig. 1). The regional averages of aerosol particle size distribution, composition and optical properties are based on data from straight level runs sampling the regional haze. Data sections corresponding to plume penetrations (identified from spikes in CO, CO2, BC and aerosol scattering) were filtered out prior to averaging. An overview of the flights and full details of instrumentation are provided in Darbyshire and Johnson (2012) and data processing methods will be described in Darbyshire et al. (in preparation, 2016). Aircraft measurements have also been taken from the Dust and Biomass Burning Experiment (DABEX) over West Africa (7-15°N, 0-7°E) during Jan-Feb 2006 (Haywood et al., 2008; Johnson et al.; 2008) and from the Met Research Flight C130 aircraft during the Southern African Regional Science Initiative (SAFARI-2000) in Sept 2000 (Haywood et al. 2003) (15-25°S, 8-18°E). Similarly, we use the regional averages for aged regional haze provided from these campaigns. The boxes in Fig. 1 indicate the regions where the flights took place and where model data was averaged.

Common to each of the aircraft datasets is the use of a wing-mounted Passive Cavity Aerosol Spectrometer Probe (PCASP) to measure aerosol particle size distributions, a TSI three wavelength nephelometer (440, 550, 700nm) to measure aerosol scattering, and a single wavelength Particle Soot Absorption Photometer (523nm) to measure aerosol absorption and the SSA (when combined with the nephelometer). During SAMBBA the PCASP suffered some instrument / electronic processing errors after the first four flights (B731-734). Therefore, stringent quality checks on the data were employed to filter out affected data. After this, approximately 16 hours of PCASP data were available from 8 flights, with 75 % of this from the first four flights (B731-734) that focussed mainly on sampling aerosol dominated by biomass burning emissions. During SAMBBA, PCASP measurements of aerosol size distribution were supplemented by a GRIMM Optical Particle Counter (OPC), and a TSI Scanning Mobility Particle Sizer (SMPS). The aerosol composition was also measured during SAMBBA and DABEX. In both cases the sulphate mass and the Organic Aerosol (OA) (i.e. total carbonaceous aerosol mass from POM and Secondary Organic Aerosol) were measured by an Aerodyne Aerosol Mass Spectrometer (Capes et al., 2008; Allan et al., 2014). During SAMBBA the BC mass was estimated from a Single Particle Soot Photometer and during DABEX the BC mass was estimated from the PSAP assuming a mass absorption coefficient of 12m^2/g. For each flight campaign the aircraft observations have been averaged over all available measurements taken in biomass burning conditions to provide campaign mean BB

aerosol properties. Ground-based observations of aerosol composition have also been used based on data presented in Tiitta et al. (2014) from the Welgegund station in South Africa (Fig. 1). They used an Aerosol Chemical Speciation Monitor to measure OA and sulphate and a Multi-Angle Absorption Photometer to measure BC assuming a mass absorption coefficient of 6.6m^2/g. We take an average composition from their measurements in September 2010.

2.6 Remote sensing observations

MODIS AOD retrievals have been obtained from the Aqua satellite. In this study we use monthly mean level 3 MYD08_M3 data products and to aid the evaluation we include the AOD products from both collection 5.1 and collection 6. In the case of collection 5.1 the dark target (Levy et al., 2007, 2010) and ocean algorithms (Remer et al., 2005) have been used where coverage is available, and the Deep Blue algorithm (Hsu et al., 2004, 2006) has been used for pixels over bright land surfaces where dark-target retrievals were not available. For collection 6 the merged product (Sayer et al., 2014) has been used that combines retrievals from all three algorithms and includes various refinements to each (Sayer et al., 2013; Levy et al., 2013). Terra products were not included as drift in the calibration of MODIS Terra in the later years of our observation window may have affected the retrieved AODs (Polashenski et al., 2015). The monthly mean data has been averaged over the period 2003-2012 to create long-term monthly means.

AERONET data have also been used for direct sun retrievals of AOD and for inversion products of aerosol size distribution and optical properties. Six sites with strong biomass burning influence were selected for use in this study: Alta Floresta (Brazil), Mongu (Zambia), Ilorin (Nigeria), Chiang Mai (Thailand), Jaribu (N. Australia), and Bonanza Creek (Alaska) (Fig. 1). We used monthly mean products from the version 2 algorithm (Dubovik and King, 2000; Dubovik et al., 2006) and used level 2 products in all cases except Chiang Mai where level 1.5 data was used as level 2 data coverage was limited. Level 1.5 data is not fully cloud-screen and calibrated so may not be as reliable. Long-term monthly mean averages were calculated for 2002-2011.

2.7 Averaging methods

The aircraft in-situ observations presented in this study have been averaged over all available measurements in biomass burning dominated conditions in each campaign or campaign sub-

region, to provide representative "campaign-mean" values. The data averaging methods for SAMBBA will be described in more detail in Darbyshire et al. (in preparation, 2016). The DABEX campaign-means are taken from the observations of aged aerosol layers in (Johnson et al., 2008). SAFARI-2000 campaign-means are based on a compilation of aged aerosol measurements, as detailed in Haywood et al. (2003). Inevitably, aircraft flight patterns do not provide unbiased spatial and temporal sampling of the atmosphere and tend to favour sampling aerosol layers with medium-high aerosol loadings. However, by averaging over large volumes of data focussed on regional sampling these aircraft datasets can provide useful constraints on the physical, chemical and optical properties of the aged aerosol. Wherever comparisons are made with model data, they are based on the 10-year (long-term) monthly mean output from the models (September for SAMBBA and SAFARI-2000, January for DABEX). For comparison with aircraft measurements, the model data has been averaged over the latitude and longitude ranges of the relevant flight regions (boxes in Fig. 1) and over 0 – 5 km; the typical altitude range of the observed aerosol layers. For the comparison with Welgegund surface measurements model data is taken from the lowest model level of the grid box co-located with the site and for September, corresponding to the peak of the BB season in Southern Africa. For comparisons with AERONET the 10-year (long-term) monthly mean model output is selected for the gridbox co-located with the AERONET site and averaged vertically to provide column-mean aerosol properties. For MODIS the level 3 data has been further averaged to generate 10-year (long-term) monthly mean AODs at the native resolution of the atmospheric model. These are compared against the long-term mean model values without any sub-sampling of the model data on observation space-time points. Sampling biases that may arise due to the lack of sub-sampling are discussed in section 3.1.

3 Evaluation of CLASSIC and GLOMAP-mode with observations

3.1 Aerosol optical depth

3.1.1 Global AOD evaluation with MODIS

Fig. 2 assesses the contribution of biomass burning to annual mean Aerosol Optical Depth (AOD) at the global scale. Figures 2 (a-d) show the results from the scaled simulations where the BB aerosol emissions scaling factors described in section 2.3.1 have been applied. For CLASSIC the contribution of BB emissions to the total AOD (hereafter BBAOD) is

straightforward as carbonaceous aerosol originating from biomass burning emissions are represented as separate (externally mixed) species in the model (Fig. 2a). For GLOMAP-mode, aerosols from different sources are internally mixed and so BBAOD is estimated as the difference in AOD between a simulation including BB emissions and one without (Fig 2b). To aid the evaluation the annual mean AOD from MODIS Aqua collections 5 and 6 are shown in Figs 2 (g & h). Finally, results are shown (Figs. 2 g & h) for the simulations where the BB aerosol emission scaling factors described in section 2.3.1 were not applied.

The results show that biomass burning dominates the annual mean AOD over S. America and Central to Southern Africa, even though BB emissions are highly seasonal in these regions. Biomass burning also makes strong contributions to annual mean AOD in parts of Indonesia, South East Asia, and Northern Australia and to a less extent the Boreal forests of N. America and North East Asia. Globally BBA emissions account for 10 % of the total AOD in the scaled CLASSIC simulation and 12 % in the scaled GLOMAP-mode simulation. The spatial distributions of BBAODs are very similar in both models, which is not surprising since they are driven by the same physical model and emission dataset. The magnitude of BBAOD is also very similar in both models as BB aerosol emissions were scaled separately in each model to ensure the modelled AOD approximately matched MODIS and AERONET AODs observed over the main BB source regions during peak BB months where BB was the dominant contributor to modelled AOD.

The impact of the BB aerosol emission scaling factors is shown by comparing the total modelled AOD from scaled and unscaled simulations. The emission scaling factors have a relatively modest impact on the global distribution of AOD when assessed on an annual mean basis. This is due to the highly seasonal nature of BB emissions. Nevertheless, even in annual means, it is clear that AODs over tropical South America and Africa are somewhat lower than observed (from both MODIS collection 5 and 6) in the un-scaled simulations. The scaling factors bring modelled AOD closer to the observations, although the benefit is clearer in later figures (3 – 5).

A wider assessment of simulated AOD from GLOMAP-mode in HadGEM3 / GA7 is expected in a future study but we note from Fig. 2 that GLOMAP-mode has improved the distribution of AOD in several regions compared to simulation with CLASSIC. For instance, it has reduced the low bias over high latitude continents (as found previously in Bellouin et al., 2013) and reduced a high bias in the southern ocean associated with sea salt aerosol. The

AOD over the Sahara and North African Atlantic coast and Arabian Peninsula appear too low in the simulations indicating that mineral dust emissions may have been too weak (in both cases simulated by CLASSIC). We note however that the GLOMAP-mode simulation also overestimates AOD in south-east Europe and eastern parts of USA which are dominated by anthropogenic sources of sulphate. A strong caveat in these comparisons is that the modelled AOD has not been sampled with the spatial and temporal incidence of the MODIS data. Schutgens et al. (2015) showed that this can result in considerable regional biases between modelled and observed monthly and annual mean AOD. In particular, the comparison may be of limited value at high latitudes (beyond 60^{o}N or S) where retrievals are not possible for several months of the year (due to solar zenith angle being too high, or due to lack of solar illumination altogether). Some degree of sampling bias may occur in regions that are frequently overcast with cloud cover (e.g. marine stratocumulus regions including the South-East Atlantic). The modelled AOD has however been calculated based on the clear-sky relative humidity to avoid strong humidification biases in partially cloudy grid boxes.

3.1.2 Seasonal AOD in biomass burning regions with MODIS

Figs 3 and 4 focus on the contribution of biomass burning to AOD in the tropical regions. Fig. 3 shows the monthly mean BBAOD and AOD for September when BB emissions peak in the Southern Hemisphere and equatorial regions. Fig. 4 shows the same for West African region but for January when BB emissions peak in the zone 5 – 15^{o} N. As in the global picture (Fig. 2) the simulations give very similar regional distributions of BBAOD and AOD. Over the BB regions the modelled AOD is generally underestimated in the un-scaled simulations compared to MODIS. In the scaled simulations total AODs agree very well with MODIS, especially over South America and Indonesia. However, some discrepancies between modelled and observed AODs remain over northern and southern parts of Africa. Firstly, the magnitude of AOD in the plume over the South-East Atlantic is lower in the models than in MODIS, even in the scaled simulations (Fig. 3). It is not clear if this is due to poor model performance or biases related to limited temporal sampling by the satellite over the marine stratocumulus region (personal communication Andrew Sayer). MODIS collection 5 and collection 6 in particular, show a large contrast in AOD between the plume over the ocean and the AOD over adjacent land areas of Southern Africa. Secondly, in Fig. 4 the peak AOD and BBAOD in the models during January are centred over central Africa (Congo basin) rather than over the Gulf of Guinea where MODIS AOD peaks. This leads to an overestimate of modelled AOD over

central Africa in the scaled simulations. Again, high cloud cover limits the spatial sampling over the Congo basin and may affect the mean AOD retrieved from MODIS. This regional bias was noted in previous modelling studies with GFED2 (Myhre et al., 2008; Johnson et al., 2008a) and may suggest there is still an underestimation in West Africa (Liousse et al., 2012) and potentially an overestimation of BB aerosol emissions in the Congo basin. The comparison of modelled and observed AOD over the BB regions of the Sahel (north of 10^{o}) is less straightforward as mineral dust aerosol contributes strongly to the total AOD.

In the remainder of this study we assess results from the simulations where total BB aerosol emissions have been scaled, as described in section 2.3.1.

3.1.3 AOD comparison with AERONET

To aid the evaluation of modelled AOD, six AERONET sites have been selected representing locations that are strongly affected by seasonal biomass burning. Once again, due to the scaling of total BB aerosol emissions both CLASSIC and GLOMAP-mode give very similar AOD and BBAOD at these locations during peak months (Fig. 5). The seasonal cycle and peak AODs seem well captured at Alta Floresta (Amazonia) and Mongu (Southern Africa). The comparison at Ilorin (West Africa) shows the model does not capture the observed seasonal cycle of AOD with a low-bias in AOD from Nov - April. This again suggests an under-representation of BB emissions across West Africa during Northern hemisphere winter, although the low-bias could be partly caused by a low-bias in mineral dust aerosol from the Sahara. The secondary peak during June-Sept, which is not shown in the AERONET observations, may be due to overestimation of BB aerosol emissions from the Congo basin and long-range transport to West Africa. BBAOD appears to be underestimated at Chiang Mai (South East Asia) and Jaribu (Northern Australia), perhaps by a factor of 2, but slightly overestimated at Bonanza Creek (Alaska). Whilst these results give clues as to where BB aerosol emissions may be over or under estimated the differences between modelled and observed AOD may be affected by various other sources of uncertainty in the models and measurements. In particular, temporal sampling biases may affect the results (Schutgens et al., 2015) as we have not sampled the model data to match AERONET retrieval times. The approach we have taken is to average over 10-years of data to gain more confidence in the long-term monthly means. The standard error on the monthly means AODs are generally much smaller than the differences between observed and modelled values, indicating that our

results are not strongly biased by interannual variability of either the simulated or observed AOD. There main exceptions are for August at Bonanza Creek and Aug – Sept at Alta Floresta where the larger standard error in AERONET AOD indicates that interannual variability has a strong impact on the comparison.

3.2 Aerosol composition

Fig. 6a and b show the column loading of fine-mode aerosol mass from the model simulations across the tropical regions during September. This is the sum of Black Carbon (BC), Organic Aerosol (OA) and sulphate (SU) from all anthropogenic and natural sources but excluding the coarse-mode contribution from GLOMAP. Clearly the fine-mode aerosol is dominated by BB sources over Africa, South America, Indonesia and Northern Australia. Figs 6 c–h show the relative contributions of OA, BC and SU to this fine-mode mass. CLASSIC and GLOMAP-mode give very similar spatial distributions for the modelled fine-mode aerosol mass loading and composition. OA clearly dominates the fine-mode aerosol mass (Fig. 6c and d) in both models across most of the region shown, where BB emissions dominate the aerosol loading. The two exceptions are the northern edge of the domain and some stretches along the Pacific coast of South America where sulphates dominate due to anthropogenic emissions of SO_2. In Fig 6 stipples mark grid columns where over 75 % of the fine-mode aerosol mass originates from BBA emissions, based on the speciation in the CLASSIC simulation. These mark the main BB plumes from S. America, Africa and Indonesia. In GLOMAP-mode where aerosols internally mix the origin of the aerosol in a grid cell can not be traced to its emission source but it seems reasonable to assume that the grid cells strongly influenced by BB emissions in CLASSIC will also be strongly influenced by BB emissions in the GLOMAP-mode given that the simulation are driven with the same emissions data and physical model configuration. The similarity in the spatial distribution of BBAOD (Fig. 2 – 4) and aerosol composition (Fig. 6) between the two models support this assumption. The same areas are therefore marked with stipples in the GLOMAP-mode plots. The mean values beneath each plot indicate the mean from the stippled areas.

In the main BB plumes (marked by stippling) the CLASSIC simulations show a slightly higher mass fraction of OA and a slightly lower mass fraction of BC compared to GLOMAP-mode with BC mass fraction averaging 5.1 % in CLASSIC and 7.2 % in GLOMAP-mode (Fig. 6e and f). These differences are due to differences in the way that BB composition is represented in the two schemes. In CLASSIC the ratio of BC to OA in the BBA species is

specified, whereas in GLOMAP-mode it varies depending on the BC and OC mass provided by the emissions data, and the OC to POM ratio assumed in the model (currently 1.4). In GLOMAP-mode Secondary Organic Aerosol (SOA) is also added interactively via the oxidation and condensation of organic vapours from bVOCs. This decreases the BC mass fraction in North Western Amazonia compared to South Eastern Amazonia and Southern Africa. In CLASSIC bVOCs are not modelled explicitly but SOA has been included using a biogenic aerosol climatology. This increases the OC mass, particularly over tropical forests, and therefore leads to a lower BC mass fraction over tropical forests compared to Savannah regions. The localized peak in BC mass fraction near to Lake Victoria in the CLASSIC simulation is due to local anthropogenic BC emissions rather than BB emissions. This shows up less in GLOMAP-mode as the regional loading of BC from BB sources is higher.

In situ measurements from three observation campaigns have been used to evaluate the aerosol composition in the simulations. The observations include FAAM aircraft measurements from Western Amazonia (Rondonia) and Eastern Amazonia (Tocantins) during SAMBBA (Darbyshire et al., in preparation, 2016), ground-based observations from the Welgegund measurement station in South Africa (Vakkari et al. 2014), and FAAM aircraft measurements from West Africa during DABEX (Capes et al. 2008). Fig. 7 compares the observed and modelled aerosol composition by plotting the relative contributions from BC, OA and sulphate to the total fine-mode aerosol. Nitrate, dust and sea salt have been excluded from the analysis as nitrate was not available in the model simulations and accurate measurements of dust and sea salt were not readily available from all observation campaigns. Given that these components are neglected we can not provide a full analysis of the aerosol composition here. The purpose of Fig 7 is rather to examine whether the relative proportions of BC, OA and sulphate are in-line with the observational evidence (as these are the dominant contributors to fine-mode mass and fine-mode AOD in the simulations).

In all cases the fine-mode aerosol is dominated by OA with modest contributions from sulphate and generally a smaller contribution from BC. On the whole the models are able to capture the typical make-up of the aerosol and some of the variations with region, such as the higher contribution from sulphates in South Africa. GLOMAP-mode gives slightly higher BC mass fractions than CLASSIC and in general GLOMAP-mode BC mass fractions are closer to observed values. Modelling the BC mass fraction is of key importance for estimating absorption and the sign of direct radiative forcing. Tentatively, GLOMAP-mode therefore

shows some improvement over CLASSIC, although it still appears to underestimate BC mass fraction relative to the measurements from West Africa, Eastern Amazonia, and to a lesser extent in South Africa. However, the use of the filter based absorption measurements in those datasets may lead to a significant overestimation of observed BC mass (Lack et al., 2008). Also, note that different mass absorption coefficients were assumed in the analyses of the DABEX ($12 m^2/g$) and Welgegund ($6.6 m^2/g$) observations. Unifying this assumption to an intermediate value of $10 m^2/g$ would change the estimated BC mass fraction to 14.1 % for DABEX and 8.2 % for Welgegund.

3.3 Size distributions

3.3.1 Comparison with aircraft data

Fig. 8 shows the size distributions from the models and in situ observations from the three aircraft campaigns. The CLASSIC curve is simply the size distribution given by the average mixture of fresh and aged BBA species in the model. Each of these CLASSIC modes is represented by a single log-normal. Both modes have a small standard deviation of 1.3 and the mean diameters are 0.2 μm for the fresh mode and 0.24 μm for the aged mode. Combining these gives a fairly narrow distribution peaking in the accumulation mode. The GLOMAP-mode size distribution is the sum of all five modes (nucleation, Aitken soluble and insoluble, accumulation soluble, coarse soluble). Each campaign includes data from a common PCASP instrument but SAMBBA included a GRIMM OPC behind a low-turbulence inlet and a Scanning Mobility Particle Sizer (SMPS). These instruments provide a dry aerosol size distribution as heating tends to the remove water from the measured aerosol samples. The three instruments from SAMBBA are in good agreement regarding the shape of the accumulation mode and the rate of decline from the accumulation to coarse mode (0.3 – 1 μm). To avoid mismatches from sampling different total concentrations, the PCASP size distributions have been normalized to give a total concentration of unity, and other observed and modelled curves have been normalized to match the peak amplitude of the PCASP.

The dry particle size distribution simulated by GLOMAP-mode is shown in Fig. 8 and matches the observed size distributions remarkably well. The broad peak in aerosol number around 0.2 μm and the rate of decline either side of the peak seem well supported by the available observations. The discrepancies between the GLOMAP-mode and observed size distributions across the coarse mode (D > 1 μm) are most likely because mineral dust is not

represented in this version of the modal scheme (this is certainly the reason in the DABEX case; Fig. 8b). Another potential issue in the Amazon case is the absence in the model of any representation of primary biological aerosol particles which may contribute significantly to the observed coarse mode in this forested region (e.g. Scot et al., 2012), though such particles are only likely to be important in the surface mixed layer. Also, measurements of low concentrations of super-micron particles will have bigger uncertainties than measurements of the accumulation–mode peaks. The agreement between GLOMAP-mode and the observations across the accumulation mode (0.1 – 0.6 μm) is partly due to a well chosen initial size distribution that is assumed for primary emissions of BBA (this a log-normal with a mean diameter of 0.15 μm and standard deviation of 1.59 as used by Stier et al., 2005). This sets the mass and number of particles emitted into the Aitken insoluble mode. Subsequently, as a result of ageing these particles grow and are transferred to the accumulation soluble mode, where most of the BC and OA mass ultimately resides. Here coagulation and condensation create an internal mixture of sulphate, sea salt, OC, BC and water from all modelled sources. The combination of a well chosen initial size distribution for the primary emissions, and subsequent microphysical and chemical processes operating through the modal framework, are therefore very successful in predicting the aerosol size distribution over BB regions.

CLASSIC provides a reasonable representation of the aerosol size distribution through the centre of the accumulation mode (0.1 – 0.6 μm) that is most important for optical properties in the visible and near-infrared spectrum. CLASSIC naturally fits the SAFARI-2000 PCASP observations (Fig. 8c), on which it was originally based (Haywood et al. 2003), but also fits the DABEX and SAMBBA observations reasonably well across the intended size range.

It is interesting to note that the observed size distributions do not vary greatly across the accumulation mode (0.1 – 0.6 μm) between the three BB campaigns. These campaigns span three of the main continental source regions of BBA (Fig. 9a) and include a range of biomes and fire conditions. This finding of little variation in size distribution between different biomass burning source regions suggests the approach of using a globally representative size distribution in CLASSIC, and of using a single “emission size distribution” for all primary biomass burning emissions in GLOMAP-mode is a reasonable approximation. We note however that Dentener et al. (2006) present a synthesis of observations from a wider collection of observations, suggesting considerable variation in size distribution (their Figs. C1 and C2). These indicate apparently large changes in physical and optical properties

between different biomass burning source regions and/or following ageing of plumes. The large differences shown in Dentener et al. (2006) could in part be related to differences in systematic biases or sizing corrections applied to differences instruments, while here we present coherent results from essentially the same instrument (Fig 9b).

3.3.2 Comparison with AERONET size distributions

In Fig. 10 AERONET retrievals of particle size distribution are used as an additional constraint to assess the modelled aerosol size distribution. These are given in terms of particle volume across the fine and coarse modes (0.1 – 15 µm) and all distributions have been normalized to give peak amplitudes of 1. The overall shape of the distribution varies very little from year to year (Fig 10a) with a dominant fine-mode peaking around 0.3 µm. The relative contribution from coarse-mode particles varies from year to year but is generally small. A similar analysis was performed for Mongu and produced an almost identical fine-mode size distribution giving some confidence that Alta Floresta is representative for tropical biomass burning regions.

Fig. 10b compares the AERONET size distribution to the PCASP and GRIMM OPC aircraft instrument data from the Western SAMBBA region. Again, all size distributions have been normalized to give the same peak amplitude. It is encouraging that the PCASP gives an almost identical size distribution to AERONET across the fine-mode. The GRIMM OPC size distribution covers only a portion of the fine-mode size range but the data are consistent with the existence of a peak at 0.3 µm, a minimum around 1 µm and a peak at coarser sizes. The aircraft instruments do not agree so well with AERONET on the amplitude or diameter of the coarse mode. The coarse-mode could be a mixture of mineral dust, primary biogenic particles or fly ash from BB (Martin et al., 2010). Sampling issues (e.g. altitude) may be a large source of representativeness error in the PCASP and GRIMM measurements of super micron particles. However, the coarse-mode is not the focus of the assessment here as the sources are unclear and it contributes very little (5 – 10 %) to the AOD or optical properties.

Fig. 10c compares the mean AERONET size distribution with the models. For CLASSIC the size distribution of the BBA species is plotted whereas GLOMAP-mode is the column-mean for September co-located with Alta Floresta. Both modelled size distributions peak at about the same diameter (~0.3 µm) as AERONET. The CLASSIC size distribution is a little narrower than AERONET whereas GLOMAP-mode predicts about the same width as

AERONET. This increases confidence that GLOMAP-mode is able to predict aerosol size distributions accurately, and is an improvement over the specified distribution in CLASSIC.

3.4 Optical properties

In this section the aerosol optical properties from the models are compared and evaluated against AERONET retrievals and in-situ measurements from aircraft campaigns. The methods for deriving optical properties are described below and results are then discussed separately for each optical property.

Firstly the column-average moist aerosol properties have been calculated from the models to assess how these vary regionally in the two aerosol schemes. The fine-mode specific extinction coefficient ($k_{ext,fm}$) (Fig. 11a & b) was calculated as the ratio of fine-mode moist AOD to fine-mode dry aerosol mass. In GLOMAP-mode the fine-mode includes the Aitken soluble, Aitken insoluble and accumulation-soluble modes. In CLASSIC the fine-mode is taken to include all sulphate and carbonaceous aerosol species. The Single Scattering Albedo (SSA) (Fig.11c & d) has been calculated from the AOD and Absorption-AOD (AAOD) at 550nm, and the Ångström exponent (Å) (Fig. 11e & f) is calculated from the wavelength dependence of AOD across 440 – 670nm. The stipples in Fig. 11 mark grid columns where over 75 % of the fine-mode aerosol mass originates from BBA emissions (as in Fig. 6, based on CLASSIC speciation) and the mean values beneath each plot indicate the mean from the stippled areas.

Secondly, the modelled SSA and Å are compared for all months against AERONET retrievals for Alta Floresta and Mongu (Fig. 12). Monthly mean SSA retrievals were not available in all months of the year due to low temporal sampling frequency outside of the dry season (inversions require AOD > 0.4 and cloud-free skies). In addition to AERONET level 2 criteria we only accept a monthly mean if data were available from at least 3 separate days in that month, and only calculate the long-term monthly mean if at least 3 monthly means were available in the time series. The AERONET retrievals of Å relied on direct sun measurements of AOD at 440 and 670nm and have better temporal sampling enabling long-term monthly means to be calculated for every month.

Finally, Table 2 compares dry aerosol optical properties of SSA, Å, $k_{ext,fm}$, and asymmetry parameter (g) from the models and from the mean values from the aircraft campaigns (references provided in the table). The comparison is made for dry aerosol since heating tends

to dry the aerosol samples measured by the aircraft instruments. For CLASSIC, the optical properties are specified and so values in Table 2 are simply derived by averaging together the optical properties for fresh and aged BBA species, based on the typical mixture simulated over the BB regions (10 % fresh, 90 % aged). For GLOMAP-mode the dry optical properties in Table 2 were calculated from Mie theory using the dry size distribution and refractive index for each of the fine modes (Aitken soluble, Aitken insoluble and accumulation-soluble) and then averaged across the modes weighting by total extinction (or by scattering for g).

3.4.1 Fine-mode specific extinction coefficient (kext,fm)

The fine-mode moist specific extinction (Fig. 11a & b) varied quite widely in both models but was generally higher in GLOMAP-mode, especially in areas where sulphates were more dominant (see Fig. 6h). This is due to a high water uptake by sulphate in the current GLOMAP-mode configuration. In the main BB plumes (marked by stipples), where OA dominates the aerosol mass, the values of $k_{ext,fm}$ range from 5 – 10 m^2/g with the highest values in both models over the moister regions of Indonesia and the lowest values in Southern Africa where the average relative humidity was lower in the lower troposphere (not shown). The average values from the BB plumes (stippled areas) are fairly similar with slightly lower value of 6.2 m^2/g for CLASSIC and a value of 6.9m^2/g for GLOMAP-mode. Note these values are indicative of the aerosol mixture as a whole rather and so are affected by the representation of other aerosols also. In Table 2 the dry values of $k_{ext,fm}$ are similar for CLASSIC (5.0 m^2/g) and GLOMAP-mode (4.5 – 4.8 m^2/g) and are within the range given by the aircraft measurement campaigns (3.6 – 5.8 m^2/g). Note, in this case the dry value given for CLASSIC corresponds to the BB species only.

3.4.2 Single scattering albedo (SSA)

The SSA of aerosol over BB dominated regions was generally lower in GLOMAP-mode than in CLASSIC for both the ambient (moist) values (Fig. 11c and d; Fig. 12a and c) and dry values (Table 2). This is consistent with the higher BC mass fraction in GLOMAP-mode (Fig 7). The lower dry SSA values from GLOMAP-mode (0.85 – 0.87) agree better with the range from the aircraft campaigns (0.79 – 0.88) than CLASSIC (0.91). The ambient SSA values from GLOMAP-mode during the dry season (July – Oct) (0.87 – 0.94) also agree better with AERONET observations from Alta Floresta and Mongu (Fig. 12a and c). The ambient SSA also shows a high degree of spatial variability in both models (Fig. 11c and d). These

variations are mainly caused by variability of composition and water content. As shown in section 3.5 the hygroscopic growth may be overestimated in both models so the spatial variation of ambient SSA and its relation to humidity may not be entirely realistic. However, the AERONET observations do show a contrast between the drier region of Southern Africa (represented by the Mongu site in Fig. 11c) where the long-term monthly mean SSA drops to 0.82 – 0.85 during July – September, and the moister Amazonian region (represented by the Alta Floresta site in Fig. 11a) where the long-term monthly SSA is around 0.92 during August – September. This observed variation may be explained more by variations in BC content rather than due to variations in hygroscopic growth. There is likely a higher BC content in the aerosol column over Mongu due to the drier vegetation burning more through flaming combustion (some evidence for the higher BC content is found in Fig. 7d for the Welgegund observations that are in the same continental region).

3.4.3 Ångström exponent (Å)

The CLASSIC aerosol scheme gives a fairly high Ångström exponent with a dry value of 2.3 for the BBA species (Table 2), and moist values of 1.9 – 2.1 for the fine-mode aerosol mixture over BB dominated regions (Fig. 11e). This is due to the fairly narrow size distribution assumed in CLASSIC. These values of Å are somewhat outside the observed range from the aircraft campaigns (dry values of 1.7 – 2.1 from nephelometer measurements) and AERONET (long-term monthly mean moist values of 1.7 – 1.9). GLOMAP-mode gives slightly lower values of Å than CLASSIC, with dry values ranging from 2.0 – 2.1 (Table 2), and ambient (moist) values ranging from 1.5 – 1.9 over the BB regions (Fig. 11f). These agree quite well with the aircraft observations and AERONET observations during the peak of the burning season (Aug-Sept) (Fig. 12b and d). The seasonal variation of Å observed by AERONET (i.e. the drop to lower values outside the burning season in Fig. 12b & d) is not well captured in either model. This could be due to insufficient representation of coarse particles, such as mineral dust or primary organic particles outside the BB season.

3.5 Hygroscopic growth

The hygroscopic growth of aerosol (i.e. the growth of the aerosol with relative humidity due to the uptake of water) leads to enhanced scattering. This can be expressed via the scattering growth factor (GF_{sca}), which is the observed or modelled scattering of the aerosol at ambient humidity divided by the scattering of the same aerosol when completely dried (i.e. at very low

relative humidity). For CLASSIC the hygroscopic growth is specified via an empirical fit that reproduces the GF_{sca} curve observed by Magi and Hobbs (2003), hereafter MH03. In MH03 GF_{sca} curves were derived from a humidified nephelometer system operated on flights over Southern Africa during SAFARI-2000. MH03 parameterized the GF_{sca} curves for a range of aerosol conditions and the CLASSIC scheme uses their "heavy smoke" curve for the fresh BBA species, and their "regional air" curve for the aged BBA species. These GF_{sca} curves are shown on Fig 13, along with a representative curve for CLASSIC assuming a mixture with 10 % fresh BBA and 90 % aged BBA. These give a very strong increase of scattering with RH for the CLASSIC BBA, with GF_{sca} rising to 2.05 at 80 % and to 3.4 at 100 %. With similar instrumentation Kotchenruther and Hobbs (1998), hereafter KH98, found much lower GF_{sca} for BB dominated aerosol over Brazil (Fig. 13). For RH > 65 % the range from KH98 does not overlap that from MH03, and at 80 % the range from KH98 is only 1.05 – 1.29. The large difference between these two observation sets is difficult to reconcile, especially as both were derived from an airborne humidified nephelometer system. Possibly the regional aerosol mixture (categorised as "regional air" in MH03) contained a substantial proportion of highly hygroscopic sulphate from industrial sources in Southern Africa and is therefore not representative of purely carbonaceous aerosol.

Additional constraints on hygroscopic growth have been provided more recently from Hygroscopic Tandem Differential Mobility Analyzer (H-TDMA) instruments. A wide range of measurements, including Amazonian aerosol are summarized in the review of Swietlicki et al. (2008). More recent measurements for Amazonia are also provided in Whitehead et al. (2014). In these analyses the hygroscopic growth is summarized via the "kappa" parameter (κ) that can be used to reconstruct the growth curve from Kohler theory. Swietlicki et al. (2008) give a range of κ values of 0.05 – 0.15 for Amazonian dry season / BB conditions, leading to GF_{sca} of 1.16 – 1.49 at 80 %. The Kohler curves based on this range of κ are also plotted in Fig. 13. For RH < 90 % the Kohler curves provide an intermediate range of growth factors that overlap the upper range from KH98 and the lower range from MH03. However, the Kohler curves have greater curvature and rise very steeply for RH > 80 % and exceed the range from MH03 for RH > 95 %. This reflects the increasing level of uncertainty in GF_{sca} at higher RH where growth factors become increasingly difficult to verify from the observations. Both the empirical fits in KH98 and MH03, and the theoretical Kohler curves are essentially extrapolated from the observed growth up to 80 % or 90 %.

For GLOMAP-mode the hygroscopic growth curve is calculated based on the Zdanovski-Stokes–Robinson (ZSR; Stokes and Robinson, 1966) mixing rule. For this comparison we take the average fine-mode composition from the four regions / sites in Fig 7, which gives a mixture with 82.6 % organic carbon, 9.4 % sulphate, and 8 % black carbon. The black carbon is assumed to be hydrophobic whereas organic carbon is assumed hydrophobic when in the Aitken insoluble mode (where approximately one third of the OA resides) and hygroscopic in the soluble modes (most of the remaining two-thirds of OA). The water uptake by soluble OA is based on sulphuric acid but scaled down such that the carbonaceous aerosol from BB takes up approximately 25 % of the water of an equivalent dry mass of H_2SO_4. The GF_{sca} curve in GLOMAP-mode is capped at a RH of 90 % to avoid overestimation of aerosol scattering and AODs close to saturation. For relative humidity above 60 % GLOMAP-mode gives lower GF_{sca} than CLASSIC, with GF_{sca} reaching 1.66 at 80 % and 2.19 for 90-100 % (compared to 2.1 and 2.6 – 3.4 for CLASSIC). For RH < 60 % GLOMAP-mode has a slightly higher GF_{sca} than CLASSIC and has an unrealistic shape, but this is unlikely to be important compared to the difference at higher RH.

Overall, although there is large uncertainty from the observations it seems likely that the CLASSIC scheme overestimates the GF_{sca} and therefore aerosol scattering, AOD and single scattering albedo for BBA in moist conditions (e.g. RH > 60 %). GLOMAP-mode may also overestimate the hygroscopic growth, though to a lesser extent. The representation of hygroscopic growth could be improved in both aerosol schemes. One option would be to use Kohler curves with observationally constrained κ values, though care would be needed in dealing with the growth assumed at the upper RH range.

3.6 Vertical distribution of aerosol

The vertical distribution of BBA in the models depends on the vertical profile of emissions and on transport and removal processes. The emission profiles and transport processes are treated identically for the two aerosol schemes but the representation of wet and dry removal processes are different. The modelled profiles of fine-mode aerosol mass are assessed in Fig. 14 by comparing them with campaign-mean aircraft observations. For the SAMBBA and DABEX cases the observed profile of fine-mode mass has been estimated from the nephelometer measurement of dry aerosol scattering multiplied by the fine-mode specific extinction ($k_{ext,fm}$) and SSA. Due to use of a modified Rosemount inlet serving the nephelometer on the FAAM aircraft, coarse-mode particles are not well sampled. We

therefore make the assumption that the total nephelometer scattering serves as a reasonable guide to fine-mode aerosol concentration. For the conversion of scattering to fine-mode mass we take the $k_{ext,fm}$ and SSA values derived from the in-situ aircraft observations in Table 2. For SAMBBA (Fig. 14a) the campaign mean profile is representative of the Western Amazonia region around Porto Velho, Rondonia. The aerosol extinction coefficient derived from the airborne lidar in SAMBBA was also averaged over a range of flights observing regional BBA layers in the Amazonian region (Marenco et al., 2015). The lidar-derived extinction at 355nm was converted to dry extinction at 550nm using an Ångström exponent of 1.7 based on the AERONET September monthly mean at Alta Floresta (Fig. 12a), and the average humidity growth factor from KH98 (Fig. 13). For DABEX the campaign mean profile is taken from Johnson et al. (2008a) and included a correction to subtract the scattering associated with mineral dust aerosol. For SAFARI-2000 no campaign mean profile was available but Haywood et al. (2003) provides information on the observed range of heights for the elevated layers observed over the South East Atlantic. To indicate the degree of sampling error in the mean profiles the standard error is also shown in Fig. 14 for both the observations and models. For the observations the standard error has been calculated as the standard deviation of aerosol mass at a given altitude divided by the square root of the number of profiles (for the nephelometer) or flight sections (for the lidar). For the models the standard error is calculated as the standard deviation from the ten monthly mean profiles in each simulations, divided by the square root of ten (the number of years).

The two models predict very similar vertical distributions of fine-mode aerosol with approximately the same profile shape and magnitude of aerosol mass. In most places differences between the models are comparable to the standard error associated with interannual variability. The models also agree quite well with the observations in terms of reproducing the basic vertical structure and profile shape. Over Amazonia the observed profile shows a fairly well mixed layer up to 1.5 km, a small increase around 1.5- 2 km and then a gradual decline from 2 – 6 km and very little above 6 km. The lidar gives a similar shaped profile to the nephelometer except with a more pronounced peak around 2 km. Although the concentrations of aerosol mass observed during SAMBBA were highly variable in space and time (Marenco et al., 2016), the relatively low standard error shows that by averaging over a sufficient sample of flight sections (lidar) or profiles (nephelometer) the campaign mean nephelometer and lidar profiles do provide a useful guide for evaluating the models. The lidar and nephelometer profiles are not expected to match exactly as the spatial

and temporal sampling frequency was different and lidar profiles are more uncertain near the ground. Both models capture the shape of the observed profiles reasonably well even showing the increase around 2 km. During DABEX the BB dominated aerosol layers were observed to reside in an elevated layer from 1.5 – 5 km with only low concentrations below. These elevated layers originated from BB emissions further south but had been undercut by Saharan air, lofted and transported north and west towards the observed region (mainly around Niamey, Niger). The models capture the elevated layer but predicted concentrations are lower than observed. During SAFARI-2000 the BB dominated aerosol over the South Eastern Atlantic were observed to reside in elevated layers with a fairly consistent layer base at 1.5 +/- 0.6 km and layer top at 4.9 +/- 0.7 km. The models both simulate an elevated layer peaking within this altitude range but with some spread above and below the observed limits of the layers. The two models give very similar vertical profiles though the mass concentration peaks at slightly higher values in CLASSIC in the centre of the layer.

Overall the results show that HadGEM3 predicts the vertical profile of BBA quite well despite the current rather crude set of assumptions for plume injection height. As detailed in section 2.3 the emissions from Savannah were injected at the surface and emissions from forest/deforestation uniformly over the lowest 3 km. More sophisticated approaches where plume injection heights are predicted online in the model should certainly be investigated, but it is encouraging that the current approach works reasonably well for the cases investigated here.

4 Conclusions

We conclude that the implementation of GLOMAP-mode has improved the representation of biomass burning aerosol in HadGEM3. The modal scheme is able to predict the full aerosol size distribution, and simulate the variation of aerosol composition and optical properties giving the scheme increased accuracy over the CLASSIC bulk scheme of HadGEM2-ES. The simulated aerosol properties, AOD and aerosol vertical distribution are shown to compare well with observations from SAMBBA and two other aircraft campaigns (DABEX, SAFARI-2000), and with remote sensing retrievals from MODIS and AERONET.

The analysis of field observations showed biomass burning aerosols to have reasonably consistent size distributions, Ångström exponents (1.7 – 2.1) and dry specific extinction coefficients (3.6 – 5.8 m^2/g) across different tropical biomass burning regions. CLASSIC represents this reasonably well by specifying a globally-representative size distribution that

includes the particle size range most important for interaction with solar radiation. GLOMAP-mode simulated the full size distribution from nucleation to coarse (0.01-10 μm), showing realistic features with good agreement against the available observations. The agreement between modelled and observed size distributions stems from a well constrained initial size distribution for the emitted particles, followed by a good representation of how this size distribution evolves with chemical and microphysical processes. GLOMAP-mode was also able to predict the optical properties with improved accuracy.

However, the analyses suggest that both aerosol schemes overestimate the uptake of water at high relative humidity. This overestimation is greater in CLASSIC and is likely to cause an overestimation of aerosol scattering, AOD and SSA in moist regions. In CLASSIC the aerosol scattering coefficient rises by a factor of 2.1 from dry conditions to 80 % relative humidity, whereas in GLOMAP-mode it rises by a factor of 1.7. Although there is considerable uncertainty and variability amongst observations, recent measurement from H-TDMA suggest lower growth factors for aged BB aerosol with the factor of increase in aerosol scattering in the region of 1.2 – 1.5 from dry to 80 % relative humidity.

The analysis of observations in this study also highlights the strong variations in black carbon (BC) mass fraction (5 – 12 %) and Single Scattering Albedo (SSA) (0.79 – 0.88) in the average biomass burning aerosol composition from different tropical source regions. These variations are a challenge for the models to capture. Whilst the dry BC mass fraction and SSA in GLOMAP-mode (7-10 %; 0.85 – 0.87) are closer to the observed values than CLASSIC (5-9 %; 0.91), the modelled variability between source regions is lower than observed. This may point to the need for a wider range of BC:OC ratios in the emissions data, which in GFED3 are based on Andreae and Merlet (2001). These have been updated in GFED4 (Giglio et al., 2013) based on Akagi et al. (2011) and future studies may provide useful feedback on whether these improve the variability of aerosol composition in models. The emissions of BBA had the same prescribed vertical profile in both models and led to very similar vertical distributions of fine-mode aerosol mass over the main tropical BB regions that compared well with the airborne in-situ and lidar observations.

Whilst both schemes gave good agreement between observed and modelled AODs over BB regions, this was achieved by scaling up the total aerosol emissions from GFED3.1 by a global scaling factor of 1.6 for CLASSIC and 2.0 for GLOMAP-mode. This might suggest that the emissions of BC and OC from GFED3 lead to an underestimate of the aerosol mass.

However, we note that there is considerable uncertainty in other parameters in the models that affect the aerosol mass and AOD from BB sources. Firstly, there is considerable uncertainty in the ratio used to convert the OC (i.e. carbon mass provided by the emissions data) to the total mass of POM emitted in the models. This depends on the ratio of carbon to oxygen and other elements in the emitted aerosol. In the current configuration of HadGEM3 CLASSIC does not account for this issue (effectively neglecting the non-carbon mass) and GLOMAP-mode converts the OC to POM using a ratio of 1.4 that is likely too low for biomass burning emissions. On the other hand CLASSIC increases the total aerosol mass by a factor of 1.62 on a 6 hour e-folding timescale to represent condensation growth during ageing (a process that GLOMAP-mode does not include). Therefore, the emission scaling factors required to generate agreement between modelled and observed AODs clearly depend on these other scaling applied within the aerosol schemes, as well as aerosol optical properties ~~and aerosol lifetime~~. For instance, the global emission scaling factor for GLOMAP-mode could be decreased from 2.0 to 1.5 if the OC to POM ratio was increased from 1.4 to around 1.9, which would still be within the range reported from observations of aerosol mixtures heavily impacted by biomass burning or wood smoke (e.g. Turpin and Lim, 2001; Aitken et al., 2008; Ng et al., 2010; Tiitta et al., 2014; Brito et al., 2014). This would reduce the black carbon emissions from BB by 25% leading to a slightly less favourable comparison of modelled chemical composition and single scattering albedo with the observations presented in this study. An upward revision to the refractive index of BC and/or the inclusion of brown-carbon absorption could be implemented to address the reduction of BC absorption. Aerosol lifetimes also clearly will affect the loading of aerosol mass and AOD, implying that the global emission scaling factors could change with the representation of aerosol removal processes and the simulation of moist processes. Other models may not require emission scaling to gain good agreement with observed AODs or may require different scaling factors outside the range 1.6 – 2.0 found in this study. Moreover, due to the difficulties of comparing large-scale models with limited observations, these scaling factors are not precise but rather indicate the approximate scale of the AOD biases. It is also worth noting that there are large differences between emission factors estimated for different measures of the aerosol mass: BC + OC, Total Carbon (TC), Total Particulate Matter (TPM), PM2.5 and PM10 (see Andreae and Merlet 2001; Akagi et al., 2011). For instance the emission factors for TPM are a factor of 2.3 – 2.4 higher than the sum of BC + OC in GFED3 (based on Andreae and Merlet 2001) for tropical BB sectors. Using TPM instead of BC and OC in our simulations would therefore

Comment [b3]: Some more substantial discussion here of how OC:POM ratios could be increased and the impacts this would have on BC mass, and absorption / SSA. This brings out the final points made in the co-editor's comments and we hope fully addresses the issue.

Note, we did not feel that the emission scaling factors could be completely as recent observations of OC:POM ratio in fresh BB plumes (refs in the text) generally have values less than 2. Higher OC:POM ratios are certainly observed in aged mixtures but we would suggest that models need to represent the ageing processes that lead to this enhanced mass.

have led to an overestimation of AOD in tropical regions unless the global emission scaling factor was reduced to approximately 0.67 in CLASSIC and approximately 1.15 in GLOMAP-mode. With such large uncertainty and observed variability in emission factors, POM:OC ratios, hygroscopic growth and secondary formation of organics, it is difficult to advocate any particular set of changes that would improve the models, though clearly there is scope to reduce the discrepancy between modelled and observed AOD without the use global emission scaling factors.

Furthermore, although tuning the emissions gave good overall agreement with observed AOD in the dominant tropical BB regions, some regional discrepancies remained. In particular, we note a low bias over West Africa and a high bias over the Congo basin during Northern hemisphere winter. The AOD over South East Asia and Northern Australia during their BB seasons were also underestimated in our simulations, but the contribution of BB to AOD in the high latitude Boreal forests seems to be slightly overestimated. Regional biases in AOD may be caused, to some extent, by regional (or biome specific) biases in the total emission rate. Other factors may include variations in aerosol optical properties between different regions (e.g. due to different size distribution or water uptake) that may not be captured in the models. Applying a globally uniform scaling factor to account for current uncertainties in BB emission datasets is therefore not sufficient to reconcile the modelled AOD with observations. GFED version 4 (Giglio et al., 2013) has already made significant progress in addressing biases related to small fires (Randerson et al., 2012) that are difficult to identify from burned area products. Follow on studies from this work are recommended to assess the impact of recent developments in fire emission modelling on reducing such regional biases.

Overall we conclude that GLOMAP-mode provides a good simulation of BB aerosol for modelling their impacts on radiation and climate. Impacts on CCN and cloud microphysics have not been evaluated here but have been assessed previously in Bellouin et al. (2013). This study does show clear improvements to the aerosol size distribution and composition in GLOMAP-mode that is important for aerosol indirect effects. This shows the benefits of including a more detailed representation of aerosol microphysical and chemistry processes. However, the model could merit from further improvements to BB processes, including more accurate estimates of the emission flux, the composition of emitted particles (which can vary considerably with vegetation / fuel type), and the injection height profile. We also note large uncertainties in the representation of hygroscopic growth, ageing, and absorption (including

the role of brown carbon). This is partly due to the complexity of these processes and difficulties in constraining them with observations.

Author contributions

J. Langridge, E. Darbyshire, W. Morgan, K. Szpeck, J. Brooke, F. Marenco contributed towards the analysis of FAAM aircraft observations from SAMBBA, J. Haywood, H. Coe, P. Artaxo, K. Longo were co-principal investigators on the SAMBBA project, J. Mulcahy, G. Mann, N. Bellouin, M. Dalvi contributed to the implementation of GLOMAP-mode aerosol scheme in HadGEM3.

Acknowledgements

The Facility for Airborne Atmospheric Measurement (FAAM) BAe-146 Atmospheric Research Aircraft is jointly funded by the Met Office and Natural Environment Research Council and operated by DirectFlight Ltd. We would like to thank the dedicated efforts of FAAM, DirectFlight, INPE, University of Sao Paulo, and the Brazilian Ministry of Science and Technology in making the SAMBBA measurement campaign possible. For AERONET data we thank the PI investigators and their staff for establishing and maintaining the sites used in this investigation (Alta Floresta and Mongu: Brent Holben, Ilorin: Rachel T. Pinker, Chiang Mai: Serm Janjai, Bonanza Creek: John R. Van de Castle, Jabiru: Ross Mitchell). We thank Andrew Sayer and Robert Levy from Goddard Space Flight Centre for their advice with MODIS aerosol products. We thank Ville Vakkari for help in selecting data from the Welgegund station. JMH, ED, WTM, HC, GM and NB were funded by SAMBBA (NERC grant NE/J009822/1). BJ, JMH and JM were funded under the Joint UK BEIS/DEFRA – Met Office Hadley Centre Climate Programme (GA01101). JMH was part funded by the IMPALA grant (NE/M017214/1) via Future Climates for Africa (FCA) funding provided by NERC and DFID.

References

Abel, S. J., Haywood, J. M., Highwood, E. J., Li, J., and Buseck, P. R.: Evolution of biomass burning aerosol properties from an agricultural fire in southern Africa., Geophys. Res. Lett.,530, 1783, 2003.

Akagi, S. K., Yokelson, R. J., Wiedinmyer, C., Alvarado, M. J., Reid, J. S., Karl, T., Crounse, J. D., and Wennberg, P. O.: Emission factors for open and domestic biomass burning for use in atmospheric models, Atmos. Chem. Phys., 11, 4039–4072, doi:10.5194/acp-11-4039-2011, 2011.

Aiken, A. C., DeCarlo, P. F., Kroll, J. H., Worsnop, D. R., Huffman, J. A., Docherty, K., Ulbrich, I. M., Mohr, C., Kimmel, J. R., Sueper, D., Sun, Y., Zhang, Q., Trimborn, A., Northway, M., Ziemann, P. J., Canagaratna, M. R., Onasch, T. B., Alfarra, M. R., Prevot, A. S. H., Dommen, J., Duplissy, J., Metzger, A., Baltensperger, U., and Jiménez, J. L.: O/C and OM/OC Ratios of Primary, Secondary, and Ambient Organic Aerosols with a High Resolution Time-of-Flight Aerosol Mass Spectrometer, Environ. Sci. Technol., 42, 4478–4485, 2008.

Allan, J. D., Morgan, W. T., Darbyshire, E., Flynn, M. J., Williams, P. I., Oram, D. E., Artaxo, P., Brito, J., Lee, J. D., and Coe, H.: Airborne observations of IEPOX-derived isoprene SOA in the Amazon during SAMBBA, Atmos. Chem. Phys., 14, 11393-11407, doi:10.5194/acp-14-11393-2014, 2014.

Andreae, M. O., Merlet, P.: Emission of trace gases and aerosols from biomass burning, Glob. Biogeochem. Cycles, 15, Issue 4, 955-966, 2001.

Andreae, M. O., Rosenfeld, D., Artaxo, P., Costa, A. A., Frank, G. P., Longo, K. M., and Silva-Dias, M. A. F.: Smoking rain clouds over the Amazon, Science, 303, 1337–1342, doi:10.1126/science.1092779, 2004.

Andres, R. J. and Kasgnoc, A. D.: A time-averaged inventory of subaerial volcanic sulfur emissions, J. Geophys. Res., 103, 25 251–25 261, 1998.

Andrews, E., Sheridan, P., Fiebig, M., McComiskey, A., et al.: Comparison of methods for deriving aerosol asymmetry parameter, J. Geophys. Res., 111, D05S04, doi:10.1029/2004JD005734, 2006.

Archer-Nicholls, S., Lowe, D., Schultz, D. M., and McFiggans, G.: Aerosol–radiation–cloud interactions in a regional coupled model: the effects of convective parameterisation and resolution, Atmos. Chem. Phys., 16, 5573-5594, doi:10.5194/acp-16-5573-2016, 2016.

Bauer, S. E., and Menon S.: Aerosol direct, indirect, semidirect, and surface albedo effects from sector contributions based on the IPCC AR5 emissions for preindustrial and present-day conditions, J. Geophys. Res., 117, D01206, doi:10.1029/2011JD016816.

Bellouin, N., Mann, G. W., Woodhouse, M. T., Johnson, C., Carslaw, K. S., and Dalvi, M.: Impact of the modal aerosol scheme GLOMAP-mode on aerosol forcing in the Hadley Centre Global Environmental Model, Atmos. Chem. Phys., 13, 3027-3044, doi:10.5194/acp-13-3027-2013, 2013.

Bellouin, N., Rae, J., Jones, A., Johnson, C., Haywood, J., and Boucher, O.: Aerosol forcing in the Climate Model Intercomparison Project (CMIP5) simulations by HadGEM2-ES and the role of ammonium nitrate, J. Geophys. Res., 116, D20206, doi:10.1029/2011JD016074, 2011.

Brito, J., Rizzo, L. V., Morgan, W. T., Coe, H., Johnson, B., Haywood, J., Longo, K., Freitas, S., Andreae, M. O., and Artaxo, P.: Ground-based aerosol characterization during the South American Biomass Burning Analysis (SAMBBA) field experiment, Atmos. Chem. Phys., 14, 12069–12083, doi:10.5194/acp-14-12069-2014, 2014.

Brooke, J. K.: Airborne Observations of the Physical and Optical Properties of Atmospheric Aerosol, PhD Thesis, School of Earth and Environment, University of Leeds, UK, 2014. Met Office CASE project.

Capes, G., Johnson, B., McFiggans, G., Williams, P. I., Haywood, J., and Coe, H.: Aging of biomass burning aerosols over West Africa: Aircraft measurements of chemical composition, microphysical properties, and emission ratios, J. Geophys. Res. Atmos., 113, D00C15, doi:10.1029/2008JD009845, 2008.

Cusack, S., Slingo, A., Edwards, J., and Wild, M.: The radiative impact of a simple aerosol climatology on the Hadley Centre climate model, Q. J. Roy. Meteorol. Soc., 124, 2517–2526, 1998.

Darbyshire, E., and Johnson B.: The South American Biomass Burning Analysis (SAMBBA) Field Experiment, Sept-Oct 2012, Brazil, Summary booklet. Available on request from the authors, 2012.

Darbyshire, E., Morgan, W. T., Allan, J., Liu, D., Flynn, M., Dorsey, J., O'Shea, S., Trembath, J., Johnson, B., Szpek, K., Marenco, F., Haywood, J., Brito, J., Artaxo, P., Longo, K., Coe, H.: Effect of fire regime on the physical and chemical properties of biomass burning aerosol over tropical South America – Perspectives from airborne in-situ observations during SAMBBA, *In preparation,* 2016.

1 Darmenov, A. and da Silva, A.: The Quick Fire Emissions Dataset (QFED) –
2 Documentation of versions 2.1, 2.2 and 2.4 NASA Technical Report Series on
3 Global Modeling and Data Assimilation NASA TM-2013-104606 version 32
4 http://gmao.gsfc.nasa.gov/pubs/docs/Darmenov609.pdf, 2013

5 Dentener, F., Kinne, S., Bond, T., Boucher, O., Cofala, J., Generoso, S., Ginoux, P., Gong, S.,
6 Hoelzemann, J. J., Ito, A., Marelli, L., Penner, J., Putaud, J.-P., Textor, C., Schulz, M., Van
7 der Werf, G. R., and Wilson, J.: Emissions of primary aerosol and precursor gases in the
8 years 2000 and 1750 prescribed data-sets for AeroCom, Atmos. Chem. Phys. Discuss., 6,
9 2703–2763, 2006, http://www.atmos-chem-phys-discuss.net/6/2703/2006/

10 Diehl, T., Heil, A., Chin, M., Pan, X., Streets, D., Schultz, M., and Kinne, S., 2012,
11 Anthropogenic, biomass burning, and volcanic emissions of black carbon, organic carbon,
12 and SO2 from 1980 to 2010 for hindcast model experiments. , doi:10.5194/acpd-12-24895-
13 2012 , Atmospheric Chemistry and Physics Discussion 12 : 24895-24954

14 Derwent, R.G., Collins, W.J., Jenkin, M.E., and Johnson, C.E., The global distribution of
15 secondary particulate matter in a 3-D Lagrangian chemistry transport model, J. Atmos.
16 Chem., 44, 57-95, 2003.

17 Dubovik, O. and King, M. D.: A flexible inversion algorithm for retrieval of aerosol
18 optical properties from Sun and sky radiance measurements, J. Geophys. Res., 105,
19 20673–20696, 2000.

20 Dubovik, O., Sinyuk, A., Lapyonok, T., Holben, B. N., Mishchenko, M.,
21 Yang, P., et al.: Application of spheroid models to account for aerosol particle
22 nonsphericity in remote sensing of desert dust, J. Geophys. Res.-Atmos., 111(D11),
23 D11208, doi:10.1029/2005JD006619, 2006.

24 Feingold, G., Remer, L. A., Ramaprasad, J., and Kaufman, Y. J.: Analysis of smoke impact
25 on clouds in Brazilian biomass burning regions: An extension of Twomey's approach, J.
26 Geophys. Res., 106, 22907–22922, 2001.

27 Freitas, S. R., Longo, K. M., Chatfield, R., Latham, D., Silva Dias, M. A. F., Andreae, M. O.,
28 Prins, E., Santos, J. C., Gielow, R., and Carvalho Jr., J. A.: Including the sub-grid scale plume
29 rise of vegetation fires in low resolution atmospheric transport models, Atmos. Chem. Phys.,
30 7, 3385–3398, doi:10.5194/acp-7-3385-2007, 2007.

1 Gao, R.S., Schwarz, J. P., Kelly, K. K., Fahey, D. W., Watts, L. A., Thompson, T.L.,
2 Spackman, R, Slowik, J.G., Cross, E.S., Han, J.-H., Davidovits, P., Onasch, T.B., and
3 Worsnop, D.R., A Novel Method for Estimating Light-Scattering Properties of Soot Aerosols
4 Using a Modified Single-Particle Soot Photometer, Aerosol Science and Technology, 41:2,
5 125-135 (2007).

6 Giglio, L., Randerson, J. T., and van der Werf, G. R.: Analysis of daily, monthly, and
7 annual burned area using the fourth-generation global fire emissions database (GFED4) J.
8 Geophys. Res. Biogeosci., 118, 317–328, doi:10.1002/jgrg.20042, 2013.

9 Guenther, A., Hewitt, C. N., Erickson, D., Fall, R., Geron, C., Graedel, T., Harley, P.,
10 Klinger, L., Lerdau, M., Mckay, W. A., Pierce, T., Scholes, B., Steinbrecher, R., Tallamraju,
11 R., Taylor, J., and Zimmerman, P.: A global model of natural volatile organic compound
12 emissions, J. Geophys. Res., 100, 8873–8892, 1995.

13 Granier, C., Bessagnet, B., Bond, T., D'Angiola, A., van der Gon, H. D., Frost, G. J., Heil, A.,
14 Kaiser, J. W., Kinne, S., Klimont, Z., Kloster, S., Lamarque, J. F., Liousse, C., Masui, T.,
15 Meleux, F., Mieville, A., Ohara, T., Raut, J. C., Riahi, K., Schultz, M. G., Smith, S. J.,
16 Thompson, A., van Aardenne, J., van der Werf, G. R., and van Vuuren, D. P.: Evolution of
17 anthropogenic and biomass burning emissions of air pollutants at global and regional
18 scales during the 1980-2010 period, Clim. Change, 109, 163–190, doi:10.1007/s10584-011-
19 0154-1, 2011.

20 Haywood, J. and Boucher, O.: Estimates of the direct and indirect radiative forcing due to
21 tropospheric aerosols: A review, Rev. Geophys., 38, 513–543, 2000.

22 Haywood, J. M., Osborne, S. R., Francis, P. N., Keil, A., Formenti, P., Andreae, M. O., and
23 Kaye, P. H.: The mean physical and optical properties of regional haze dominated by
24 biomass burning aerosol measured from the C-130 aircraft during SAFARI 2000, J. Geophys.
25 Res.-Atmos., 108(D13), 8473, doi:10.1029/2002JD002226, 2003.

26 Haywood, J. M., et al.: Overview of the Dust and Biomass-burning Experiment and African
27 Monsoon Multidisciplinary Analysis Special Observing Period-0, J. Geophys. Res., 113,
28 D00C17, doi:10.1029/2008JD010077, 2008.

29 Hewitt, H. T., Copsey, D., Culverwell, I. D., Harris, C. M., Hill, R. S. R., Keen, A. B.,
30 McLaren, A. J., and Hunke E. C.: Design and implementation of the infrastructure of

HadGEM3: The next-generation Met Office climate modelling system. Geosci. Model Dev., 4, 223–253, 2011.

Hsu, N. C., Tsay, S.-C., King, M. D., and Herman, J. R.: Aerosol properties over bright-reflecting source regions, IEEE Trans. Geosci. Remote Sens.,42 (3), 557–569, doi:10.1109/TGRS.2004.824067, 2004.

Hsu, N. C., Tsay, S.-C., King, M. D., and Herman, J. R.: Deep Blue retrievals of Asian aerosol properties during ACE-Asia, IEEE Trans. Geosci. Remote Sens., 44 (11), 3180–3195, doi:10.1109/TGRS.2006.879540, 2006.

Ichoku, C. and Ellison, L.: Global top-down smoke-aerosol emissions estimation using satellite fire radiative power measurements, Atmos. Chem. Phys., 14, 6643-6667, doi:10.5194/acp-14-6643-2014, 2014.

Johnson, B. T., Osborne, S. R., Haywood, J. M., and Harrison, M. A. J.: Aircraft measurements of biomass burning aerosol over West Africa during DABEX, J. Geophys. Res.-Atmos., 113, D00C06, doi:10.1029/2007JD009451, 2008.

Johnson, B., T., Heese, B., McFarlane, S., Chazette, P., Jones, A. and Bellouin, N.: Vertical distribution and radiative forcing of mineral dust and biomass-burning aerosols over West Africa during DABEX, J. Geophys. Res., 113, D00C12, doi:10.1029/2008JD009848, 2008b.

Johnston, F. H., Henderson, B., Chen, Y., Randerson, J. T., Marlier, M., DeFries, R. S., Kinney, P., Bowman, D. M. J. S., and Brauer, M.: Estimated Global Mortality Attributable to Smoke from Landscape Fires, Environ. Health Perspect., 120, 695–701, doi:10.1289/ehp.1104422, 2012.

Jolleys, M. D., Coe, H., McFiggans, G., Capes, G., Allan, J. D., Crosier, J., Williams, P. I., Allen, G., Bower, K. N., Jimenez, J. L., Russell, L. M., Grutter, M., and Baumgardner, D.: Characterizing the Aging of Biomass Burning Organic Aerosol by Use of Mixing Ratios: A Meta-analysis of Four Regions, Environ. Sci. Tech., 46, 13093–13102, doi:10.1021/es302386v, 2012.

Jones, A., Roberts, D. L., Woodage, M. J., and Johnson, C. E.: Indirect sulphate aerosol forcing in a climate model with an interactive sulphur cycle, J. Geophys. Res., 106, 20293-20310, doi: 10.1029/2000JD000089, 2001.

Jones, A., Haywood, J. M., and Boucher, O.: Aerosol forcing, climate response and climate sensitivity in the Hadley Centre climate model, J. Geophy. Res., 112, D20211, doi:10.1029/2007JD008688, 2007.

Kahn, R. A., Chen, Y., Nelson, D. L., Leung, F.-Y., Li, Q., Diner, D. J., and Logan, J. A.: Wildfire smoke injection heights: two perspectives from space, Geophys. Res. Lett., 35, 18–21, doi:10.1029/2007GL032165, 2008.

Kaiser, J. W., Heil, A., Andreae, M. O., Benedetti, A., Chubarova, N., Jones, L., Morcrette, J.-J., Razinger, M., Schultz, M. G., Suttie, M., and van der Werf, G. R.: Biomass burning emissions estimated with a global fire assimilation system based on observed fire radiative power, Biogeosciences, 9, 527–554, doi:10.5194/bg-9-527-2012, 2012.

Kaufman, Y. J., Hobbs, P. V., Kirchhoff, V., et al.: Smoke, Clouds, and Radiation-Brazil (SCAR-B) Experiment, J. Geophys. Res., 103(D24), 31 783–31 808, 1998.

Kettle, A., Andreae, M., Amouroux, D., Andreae, T., Bates, T., Berresheim, H., Bingemer, H., Boniforti, R., Curran, M., DiTullio, G., Helas, G., Jones, G., Keller, M., Kiene, R., Leck, C., Levasseur, M., Malin, G., Maspero, M., Matrai, P., McTaggart, A., Mihalopoulos, N., Nguyen, B., Novo, A., Putaud, J., Rapsomanikis, S., Roberts, G., Schebeske, G., Sharma, S., Sim, R., Staubes, R., Turner, S., and Uher, G.: A global database of sea surface dimethylsulfide (DMS) measurements and a procedure to predict sea surface DMS as a function of latitude, longitude and month, Global Biogeochemical Cycles, 13, 399–444, 1999.

Kolusu, S. R., Marsham, J. H., Mulcahy, J., Johnson, B., Dunning, C., Bush, M., and Spracklen, D. V.: Impacts of Amazonia biomass burning aerosols assessed from short-range weather forecasts, Atmos. Chem. Phys., 15, 12251-12266, doi:10.5194/acp-15-12251-2015, 2015.

Koren, I., Martins, J.V., Remer, L. A., Afargan, H.: Smoke invigoration versus inhibition of clouds over the amazon. Science. 2008, 321:946–9, doi:10.5194/acp-14-9641-2014, 2008.

Kotchenruther, R. A., and P. V. Hobbs, Humidification factors of aerosols from biomass burning in Brazil, J. Geophys. Res., 103(D24), 32081–32089 (1998).

Kulmala, M., Petäjä, T., Mönkkönen, P., Koponen, I. K., Dal Maso, M., Aalto, P. P., Lehtinen, K. E. J., and Kerminen, V.-M.: On the growth of nucleation mode particles: source rates of condensable vapor in polluted and clean environments, Atmos. Chem. Phys., 5, 409-416, doi:10.5194/acp-5-409-2005, 2005.

Lack, D. A., Cappa, C. D., Covert, D. S., Baynard, T., Massoli, P., Sierau, B., Bates, T. S., Quinn, P., Lovejoy, E. R., and Ravishankara, A. R.: Bias in filter-based aerosol light absorption measurements due to organic aerosol loading: Evidence from ambient measurements, Aerosol Sci. Technol., 42(12), 1033–1041, 2008.

Lamarque, J.-F., Bond, T. C., Eyring, V., Granier, C., Heil, A., Klimont, Z., Lee, D., Liousse, C., Mieville, A., Owen, B., Schultz, M. G., Shindell, D., Smith, S. J., Stehfest, E., Van Aardenne, J., Cooper, O. R., Kainuma, M., Mahowald, N., McConnell, J. R., Naik, V., Riahi, K., and van Vuuren, D. P.: Historical (1850–2000) gridded anthropogenic and biomass burning emissions of reactive gases and aerosols: methodology and application, Atmos. Chem. Phys., 10, 7017–7039, doi:10.5194/acp-10-7017-2010, 2010.

Lau, K.-M., Tsay, S. C., Hsu, C., Chin, M., Ramanathan, V., Wu, G.-X., Li, Z., Sikka, R., Holben, B., Lu, D., Chen, H., Tartari, G., Koudelova, P., Ma, Y., Huang, J., Taniguchi, K., and Zhang, R.: The joint aerosol-monsoon experiment: A new challenge for Monsoon Climate Research, B. Am. Meteorol. Soc., 89, 369–383, 2008.

Levy, R. C., Remer, L. A., Mattoo, S., Vermote, E. F., and Kaufman, Y. J.: Second-generation operational algorithm: Retrieval of aerosol properties over land from inversion of Moderate Resolution Imaging Spectroradiometer spectral reflectance, J. Geophys. Res., 112, D13211, doi:10.1029/2006JD007811, 2007.

Levy, R. C., Remer, L. A., Kleidman, R. G., Mattoo, S., Ichoku, C., Kahn, R., and Eck, T. F.: Global evaluation of the Collection 5 MODIS dark-target aerosol products over land, Atmos. Chem. Phys., 10, 103,999–10,420, doi:10.5194/acp-10-10399-2010, 2010.

Levy, R. C., Mattoo, S., Munchak, L. A., Remer, L. A., Sayer, A. M., and Hsu, N. C.: The Collection 6 MODIS aerosol products over land and ocean, Atmos. Meas. Tech. Discuss., 6, 159–259, doi:10.5194/amtd-6-159-2013, 2013.

Liousse, C., Guillaume, B., Grégoire, J. M., Mallet, M., Galy, C., Pont, V., Akpo, A., Bedou, M., Castéra, P., Dungall, L., Gardrat, E., Granier, C., Konaré, A., Malavelle, F.,

Mariscal, A., Mieville, A., Rosset, R., Serça, D., Solmon, F., Tummon, F., Assamoi, E., Yoboué, V., and Van Velthoven, P.: Updated African biomass burning emission inventories in the framework of the AMMA-IDAF program, with an evaluation of combustion aerosols, Atmos. Chem. Phys., 10, 9631-9646, doi:10.5194/acp-10-9631-2010, 2010.

Liss, P. and Merlivat, L.: The Role of Air-Sea Exchange in Geochemical Cycling, chap. Air-sea gas exchange rates: Introduction and synthesis, 113–127, D. Reidel, Norwell, Mass., 1986.

Magi, B. I. and Hobbs, P. V.: Effects of humidity on aerosols in southern Africa during the biomass burning season, J. Geophys. Res., 108, 8495, doi:10.1029/2002JD002144, 2003.

Malavelle, F., Pont V., Mallet M., Solmon F., Johnson B., Leon J.-F., and Liousse C.: Simulation of aerosol radiative effects over West Africa during DABEX and AMMA SOP-0, J. Geophys. Res., 116, D08205, doi:10.1029/2010JD014829, 2011.

Mann, G. W., Carslaw, K. S., Spracklen, D. V., Ridley, D. A., Manktelow, P. T., Chipperfield, M. P., Pickering, S. J., and Johnson, C. E.: Description and evaluation of GLOMAP-mode: A modal global aerosol microphysics model for the UKCA composition-climate model, Geosci. Model Dev., 3, 519–551, doi:10.5194/gmd-3-519-2010, 2010.

Mann, G. W., Carslaw, K. S., Reddington, C. L., Pringle, K. J., Schulz, M., Asmi, A., Spracklen, D. V., Ridley, D. A., Woodhouse, M. T., Lee, L. A., Zhang, K., Ghan, S. J., Easter, R. C., Liu, X., Stier, P., Lee, Y. H., Adams, P. J., Tost, H., Lelieveld, J., Bauer, S. E., Tsigaridis, K., van Noije, T. P. C., Strunk, A., Vignati, E., Bellouin, N., Dalvi, M., Johnson, C. E., Bergman, T., Kokkola, H., von Salzen, K., Yu, F., Luo, G., Petzold, A., Heintzenberg, J., Clarke, A., Ogren, J. A., Gras, J., Baltensperger, U., Kaminski, U., Jennings, S. G., O'Dowd, C. D., Harrison, R. M., Beddows, D. C. S., Kulmala, M., Viisanen, Y., Ulevicius, V., Mihalopoulos, N., Zdimal, V., Fiebig, M., Hansson, H.-C., Swietlicki, E., and Henzing, J. S.: Intercomparison and evaluation of global aerosol microphysical properties among AeroCom models of a range of complexity, Atmos. Chem. Phys., 14, 4679-4713, doi:10.5194/acp-14-4679-2014, 2014.

Mao, J., Horowitz, L. W., Naik, V., Fan, S., Liu, J., and Fiore, A., M.: Sensitivity of tropospheric oxidants to biomass burning emissions: implications for radiative forcing, Geophys. Res. Lett., 40, 1241–1246, doi:10.1002/grl.50210, 2013.

Marenco, F., Johnson, B., Langridge, J. M., Mulcahy, J., Benedetti, A., Remy, S., Jones, L., Szpek, K., Haywood, J., Longo, K., and Artaxo, P.: On the vertical distribution of smoke in the Amazonian atmosphere during the dry season, Atmos. Chem. Phys., 16, 2155-2174, doi:10.5194/acp-16-2155-2016, 2016.

Marlier, M. E., DeFries, S. R., Voulgarakis, A., Kinney, P. L., Randerson, J. T., Shindell, D. T., Chen, Y., and Faluvegi, G.: El Nino and health risks from landscape fire emissions in southeast Asia, Nature Climate Change, 3, 131–136, doi:10.1038/nclimate1658, 2013.

Martin, S. T., Andreae, M. O., Artaxo, P., Baumgardner, D., Chen, Q., Goldstein, A. H., Guenther, A., Heald, C. L., Mayol Bracero, O. L., McMurry, P. H., Pauliquevis, T., Poschl, U., Prather, K. A., Roberts, G. C., Saleska, S. R., Silva-Dias, M. A., Spracklen, D. V., Swietlicki, E., and Trebs, I.: Sources and properties of Amazonian aerosol particles, Rev. Geophys., 48, RG2002, doi:10.1029/2008RG000280, 2010.

Mercado, L., Bellouin, N., Stich, S., Boucher, O., Huntingford, C., Wild, M., and Wild, P.: Impacts of changes in diffuse radiation on the global land carbon sink, Nature, 458, 01014–01018, doi:10.1028/nature07949, 2009.

Morgan, W., Allan, J., Flynn, M., Darbyshire, E., Liu, D., Szpek, K., Langridge J., Johnson, B., Haywood, J., Longo, K. M., Artaxo, P., Coe, H.: Transformation of aerosol chemical composition and resultant impact on climate during the South American Biomass Burning Analysis (SAMBBA), iCACGP/IGAC-2014 Science Conference on Atmospheric Chemistry, Brazil Natal, 22-26 September, 2014.

Morgenstern, O., Braesicke, P., O'Connor, F. M., Bushell, A. C., Johnson, C. E., Osprey, S. M., and Pyle, J. A.: Evaluation of the new UKCA climate-composition model – Part 1: The stratosphere, Geosci. Model Dev., 2, 43-57, doi:10.5194/gmd-2-43-2009, 2009.

Milton, S. F., Greed G., Brooks, M. E., Haywood, J., Johnson, B., Allan, R. P., Slingo, A., and Grey, W. M. F.: Modeled and observed atmospheric radiation balance during the West African dry season: Role of mineral dust, biomass burning aerosol, and surface albedo, J. Geophys. Res., 113, D00C02, doi:10.1029/2007JD009741, 2008.

Moteki, N., and Kondo Y.: Method to measure time-dependent scattering cross-sections of particles evaporating in a laser beam, J. Aerosol Sci., 39, doi:10.1016/j.jaerosci.2007.12.002, 2008.

Myhre, G., Samset, B. H., Schulz, M., Balkanski, Y., Bauer, S., Berntsen, T. K., Bian, H., Bellouin, N., Chin, M., Diehl, T., Easter, R. C., Feichter, J., Ghan, S. J., Hauglustaine, D., Iversen, T., Kinne, S., Kirkevåg, A., Lamarque, J.-F., Lin, G., Liu, X., Lund, M. T., Luo, G., Ma, X., van Noije, T., Penner, J. E., Rasch, P. J., Ruiz, A., Seland, Ø., Skeie, R. B., Stier, P., Takemura, T., Tsigaridis, K., Wang, P., Wang, Z., Xu, L., Yu, H., Yu, F., Yoon, J.-H., Zhang, K., Zhang, H., and Zhou, C.: Radiative forcing of the direct aerosol effect from AeroCom Phase II simulations, Atmos. Chem. Phys., 13, 1853-1877, doi:10.5194/acp-13-1853-2013, 2013.

Myhre, G., Hoyle C. R., Berglen T. F., Johnson B. T., and Haywood J. M.: Modeling of the solar radiative impact of biomass burning aerosols during the Dust and Biomass-burning Experiment (DABEX), J. Geophys. Res., 113, D00C16, doi:10.1029/2008JD009857, 2008.

Ng, N. L., Canagaratna, M. R., Zhang, Q., Jimenez, J. L., Tian, J., Ulbrich, I. M., Kroll, J. H., Docherty, K. S., Chhabra, P. S., Bahreini, R., Murphy, S. M., Seinfeld, J. H., Hildebrandt, L., Donahue, N. M., DeCarlo, P. F., Lanz, V. A., Prévôt, A. S. H., Dinar, E., Rudich, Y., and Worsnop, D. R.: Organic aerosol components observed in Northern Hemispheric datasets from Aerosol Mass Spectrometry, Atmos. Chem. Phys., 10, 4625–4641, doi:10.5194/acp-10-4625-2010, 2010.

O'Connor, F. M., Johnson, C. E., Morgenstern, O., Abraham, N. L., Braesicke, P., Dalvi, M., Folberth, G. A., Sanderson, M. G., Telford, P. J., Voulgarakis, A., Young, P. J., Zeng, G., Collins, W. J., and Pyle, J. A.: Evaluation of the new UKCA climate-composition model – Part 2: The Troposphere, Geosci. Model Dev., 7, 41-91, doi:10.5194/gmd-7-41-2014, 2014.

Ott, L., Duncan, B., Pawson, S., Colarco, P. R., Chin, M., Randles, C., Diehl, T., and Nielsen, E.: The influence of the 2006 Indonesian biomass burning aerosols on tropical dynamics studied with the GEOS-5 AGCM, J. Geophys. Res., doi:10.1029/2009JD013181, D14121, 2010.

Pacifico, F., Folberth, G. A., Sitch, S., Haywood, J. M., Rizzo, L. V., Malavelle, F. F., and Artaxo, P.: Biomass burning related ozone damage on vegetation over the Amazon forest: a

model sensitivity study, Atmos. Chem. Phys., 15, 2791-2804, doi:10.5194/acp-15-2791-2015, 2015.

Petrenko, M., Kahn, R., Chin, M., Soja, A., Kucsera, T., and Harshvardhan, N.: The use of satellite-measured aerosol optical depth to constrain biomass burning emissions source strength in the global model GOCART, J. Geophys. Res., 117, D18212, doi:10.1029/2012JD017870, 2012.

Polashenski, C.M., Dibb, J.E., Flanner, M.G., Chen, J.Y., Courville, Z.R., Lai, A.M., Schauer, J.S., Shafer, M.M., Bergin, M.: Neither dust nor black carbon causing apparent albedo decline in Greenland's dry snow zone; implications for MODIS C5 surface reflectance, Geophys. Res. Letts, 10.1002/2015GL065912, 2015.

Ramanathan, V. and Carmichael, G.: Global and regional climate changes due to black carbon, Nature Geosci., 1, 221–227, doi:10.1038/ngeo156, 2008.

Ramanathan, V., Crutzen, P. J., Kiehl, J. T., and Rosenfeld, D.: Aerosols, climate, and the hydrological cycle, Science, 294, 2119–2124, 2001.

Randles, C. and Ramaswamy, V.: Absorbing aerosols over Asia:

A Geophysical Fluid Dynamics Laboratory general circulation model sensitivity study of model response to aerosol optical depth and aerosol absorption, J. Geophys. Res., 113, D21203, doi:10.1029/2008JD010140, 2008.

Rap, A., Spracklen, D. V., Mercado, L., Reddington, C. L., Haywood, J. M., Ellis, R. J., Phillips, O. L., Artaxo, P., Bonal, D., Coupe, N. R., and Butt, N.: Fires increase Amazon forest productivity through increases in diffuse radiation, Geophys. Res. Lett., 42, 4654–4662, doi:10.1002/2015GL063719, 2015.

Reddington, C. L., Butt, E. W., Ridley, D. A., Artaxo, P., Morgan, W. T., Coe, H., and Spracklen, D. V.: Air quality and human health improvements from reductions in deforestation-related fire in Brazil. Nature Geoscience 8, 768–771 doi:10.1038/ngeo2535, 2015.

Reddington, C. L., Spracklen, D. V., Artaxo, P., Ridley, D., Rizzo, L. V., and Arana, A.: Analysis of particulate emissions from tropical biomass burning using a global aerosol model

and long-term surface observations, Atmos. Chem. Phys. Discuss., doi:10.5194/acp-2015-967, in review, 2016.

Reid, J. S., Koppmann, R., Eck, T. F., and Eleuterio, D. P.: A review of biomass burning emissions part II: intensive physical properties of biomass burning particles, Atmos. Chem. Phys., 5, 799-825, doi:10.5194/acp-5-799-2005, 2005.

Reid, J. S., Eck, T. F., Christopher, S. A., Koppmann, R., Dubovik, O., Eleuterio, D. P., Holben, B. N., Reid, E. A., and Zhang, J.: A review of biomass burning emissions part III: intensive optical properties of biomass burning particles, Atmos. Chem. Phys., 5, 827-849, doi:10.5194/acp-5-827-2005, 2005b.

Remer, L., Kaufman, Y., Tanre, D., Mattoo, S., Chu, D., Martins, J., et al.: The MODIS aerosol algorithm, products, and validation, J. Atmos. Sci., 62(4), 947–973, 2005.

Reynolds, R. W., Smith, T. M., Liu, C., Chelton, D. B., Casey, K. S., and Schlax, M. G.: Daily High-Resolution-Blended Analyses for Sea Surface Temperature, J. Climate, 20, 5473–5496,doi:10.1175/2007JCLI1824.1, 2007.

Saleh, R., Robinson, E. S., Tkacik, D. S., Ahern, A. T., Liu, S., Aiken, A. C., Sullivan, R. C., Presto, A. A., Dubey, M. K., Yokelson, R. J., Donahue, N. M., and Robinson, A. L.: Brownness of organics in aerosols from biomass burning linked to their black carbon content, Nat. Geosci., 7, 647–650, 2014.

Samset, B. H., Myhre, G., Schulz, M., Balkanski, Y., Bauer, S., Berntsen, T. K., Bian, H., Bellouin, N., Diehl, T., Easter, R. C., Ghan, S. J., Iversen, T., Kinne, S., Kirkevåg, A., Lamarque, J.-F., Lin, G., Liu, X., Penner, J. E., Seland, Ø., Skeie, R. B., Stier, P., Takemura, T., Tsigaridis, K., and Zhang, K.: Black carbon vertical profiles strongly affect its radiative forcing uncertainty, Atmos. Chem. Phys., 13, 2423–2434, doi:10.5194/acp-13-2423-
2013, 2013.

Sayer, A. M., Munchak, L. A., Hsu, N. C., Levy, R. C., Bettenhausen, C., and Jeong M.-J.: MODIS Collection 6 aerosol products: Comparison between Aqua's e-Deep Blue, Dark Target, and “merged” data sets, and usage recommendations, J. Geophys. Res. Atmos., 119, 13,965–13,989, doi:10.1002/2014JD022453, 2014.

Shindell, D. T., Lamarque, J.-F., Schulz, M., Flanner, M., Jiao, C., Chin, M., Young, P. J., Lee, Y. H., Rotstayn, L., Mahowald, N., Milly, G., Faluvegi, G., Balkanski, Y., Collins, W. J.,

Conley, A. J., Dalsoren, S., Easter, R., Ghan, S., Horowitz, L., Liu, X., Myhre, G., Nagashima, T., Naik, V., Rumbold, S. T., Skeie, R., Sudo, K., Szopa, S., Takemura, T., Voulgarakis, A., Yoon, J.-H., and Lo, F.: Radiative forcing in the ACCMIP historical and future climate simulations, Atmos. Chem. Phys., 13, 2939-2974, doi:10.5194/acp-13-2939-2013, 2013.

Schutgens, N. A. J., Partridge, D. G., and Stier, P.: The importance of temporal collocation for the evaluation of aerosol models with observations, Atmos. Chem. Phys., Discuss., 15, 26191-26230, doi:10.5194/acpd-15-26191-2015, 2015.

Sofiev, M., Ermakova, T., and Vankevich, R.: Evaluation of the smoke-injection height from wild-land fires using remote-sensing data, Atmos. Chem. Phys., 12, 1995–2006, doi:10.5194/acp-12-1995-2012, 2012.

Spracklen, D. V., Carslaw, K. S., Pöschl, U., Rap, A., and Forster, P. M.: Global cloud condensation nuclei influenced by carbonaceous combustion aerosol, Atmos. Chem. Phys., 11, 9067-9087, doi:10.5194/acp-11-9067-2011, 2011.

Stier, P., Feichter, J., Kinne, S., Kloster, S., Vignati, E., Wilson, J., Ganzeveld, L., Tegen, I., Werner, M., Balkanski, Y., Schulz, M., Boucher, O., Minikin, A., and Petzold, A.: The aerosol-climate model ECHAM5-HAM, Atmos. Chem. Phys., 5, 1125–1156, doi:10.5194/acp-5-1125-2005, 2005.

IPCC: Climate Change 2013: The Physical Science Basis: Summary for Policymakers, Cambridge, UK, 2013.

Stokes, R. H., and Robinson, R. A.: Interactions in aqueous nonelectrolyte solutions, solute-solvent equilibria, J. Phys. Chem., 70(7), 2126–2131, 1966.

Swap, B., Annegarn H. J., Suttles, J. T., Haywood, J., Helmlinger M. C., Hely C., Hobbs, P. V., Holben B., Ji, J., King, M. D., Landmann T., Maenhaut W., Otter L., Pak B., Piketh, S. J., Platnick, S., Privette, J. L., Roy, D., Thompson, A. M., Ward, D., and Yokelson, R.: The Southern African Regional Science Initiative (SAFARI 2000): Overview of the dry season field campaign, S. African J. Sci., 98, 125-130, 2002.

Swietlicki, E., Hansson, H. C., Hameri, K., Svenningsson, B., Massling, A., McFiggans, G., McMurry, P., Petaja, T., Tunved, P., Gysel, M., Topping, D., Weingartner, E., Baltensperger, U., Rissler, J., Wiedensohler, A., and Kulmala, M.: Hygroscopic

properties of submicrometer atmospheric aerosol particles measured with H TDMA instruments in various environments – A review, Tellus B, 60, 432–469, 2008.

Ten Hoeve, J. E., Jacobson, M. Z., and Remer, L. A.: Comparing results from a physical model with satellite and in situ observations to determine whether biomass burning aerosols over the Amazon brighten or burn off clouds, J. Geophys. Res., 117, D08203, doi:10.1029/2011JD016856, 2012.

Tiitta, P., Vakkari, V., Josipovic, M., Croteau, P., Beukes, J. P., van Zyl, P. G., Venter, A. D., Jaars, K., Pienaar, J. J., Ng, N. L., Canagaratna, M. R., Jayne, J. T., Kerminen, V.-M., Kulmala, M., Laaksonen, A., Worsnop, D. R., and Laakso, L.: Chemical composition, main sources and temporal variability of PM1 aerosols in southern African grassland, Atmos. Chem. Phys., 14, 1909-1927, doi:10.5194/acp-14-1909-2014, 2014.

Tosca, M. G., Randerson, J. T., Zender, C. S., Flanner, M. G., and Rasch, P. J.: Do biomass burning aerosols intensify drought in equatorial Asia during El Nino?, Atmos. Chem. Phys., 10, 3515–3528, doi:10.5194/acp-10-3515-2010, 2010

Tosca, M. G., Randerson, J. T., Zender, C. S., Nelson, D. L., Diner, D. J., and Logan, J. A.: Dynamics of fire plumes and smoke clouds associated with peat and deforestation fires in Indonesia, J. Geophys. Res., 116, 1–14, doi:10.1029/2010JD015148, 2011.

Tosca, M. G., Randerson, J. T., and Zender, C. S.: Global impact of smoke aerosols from landscape fires on climate and the Hadley circulation, Atmos. Chem. Phys., 13, 5227–5241, doi:10.5194/acp-13-5227-2013, 2013.

Tosca, M. G., Diner, D. J., Garay, M. J., and Kalashnikova, O. V.: Observational evidence of fire-driven reduction of cloud fraction in tropical Africa, J. Geophys. Res. Atmos., 119, 8418–8432, doi:10.1002/2014JD021759, 2014.

Turpin, B. J., Saxena, P., and Andrews, E.: Measuring and simulating particulate organics in the atmosphere: problems and prospects, Atmos. Environ., 34, 2983–3013, 2000.

Turpin, B. J., and Lim, H. J.: Species Contributions to PM2.5 Mass Concentrations: Revisiting Common Assumptions for Estimating Organic Mass, Aerosl Sci. 35, 602–610, 2001.

Twomey, S.: Pollution and the planetary albedo, Atmos. Environ., 8, 1251–1256, 1974.

Val Martin, M., Logan, J. A., Kahn, R. A., Leung, F.-Y., Nelson, D. L., and Diner, D. J.: Smoke injection heights from fires in North America: analysis of 5 years of satellite observations, Atmos. Chem. Phys., 10, 1491–1510, doi:10.5194/acp-10-1491-2010, 2010.

Val Martin, M., Kahn, R. A., Logan, J. A., Paugam, R., Wooster, M., and Ichoku, C.: Space-based observational constraints for 1-D fire smoke plume-rise models, J. Geophys. Res., 117, D22204, doi:10.1029/2012JD018370, 2012.

Vakkari, V., Kerminen, V.-M., Beukes, J., Tiitta, P., van Zyl, P., Josipovic, M., Venter, A., Jaars, K., Worsnop, D., Kulmala, M., and Laakso, L.: Rapid changes in biomass burning aerosols by atmospheric oxidation, Geophys. Res. Lett., 41, 2644–2651, doi:10.1002/2014GL059396, 2014.

van der Werf, G. R., Randerson, J. T., Giglio, L., Collatz, G. J., Mu, M., Kasibhatla, P. S., Morton, D. C., DeFries, R. S., Jin, Y., and van Leeuwen, T. T.: Global fire emissions and the contribution of deforestation, savanna, forest, agricultural, and peat fires (1997–2009), Atmos. Chem. Phys., 10, 11707-11735, doi:10.5194/acp-10-11707-2010, 2010.

Voulgarakis, A., and Field, R. D.: Fire influences on atmospheric composition, air quality, and climate. Curr. Pollut. Rep., 1, no. 2, 70-81, doi:10.1007/s40726-015-0007-z, 2015.

Walters, D. N., Williams, K. D., Boutle, I. A., Bushell, A. C., Edwards, J. M., Field, P. R., Lock, A. P., Morcrette, C. J., Stratton, R. A., Wilkinson, J. M., Willett, M. R., Bellouin, N., Bodas-Salcedo, A., Brooks, M. E., Copsey, D., Earnshaw, P. D., Hardiman, S. C., Harris, C. M., Levine, R. C., MacLachlan, C., Manners, J. C., Martin, G. M., Milton, S. F., Palmer, M. D., Roberts, M. J., Rodríguez, J. M., Tennant, W. J., and Vidale, P. L.: The Met Office Unified Model Global Atmosphere 4.0 and JULES Global Land 4.0 configurations, Geosci. Model Dev., 7, 361-386, doi:10.5194/gmd-7-361-2014, 2014.

Ward, D. S., Kloster, S., Mahowald, N. M., Rogers, B. M., Randerson, J. T., and Hess, P. G.: The changing radiative forcing of fires: global model estimates for past, present and future, Atmos. Chem. Phys., 12, 10857–10886, doi:10.5194/acp-12-10857-2012, 2012.

World Climate Programme (WCP): Report of the experts meeting on aerosols and their climatic effects, edited by Deepak, A. and Gerber, H. G., World Meteorological Organization, Geneva, Switzerland, Rep. WCP-55, 107 pp., 1983.

Williams, K. D., Harris, C. M., Bodas-Salcedo, A., Camp, J., Comer, R. E., Copsey, D., Fereday, D., Graham, T., Hill, R., Hinton, T., Hyder, P., Ineson, S., Masato, G., Milton, S. F., Roberts, M. J., Rowell, D. P., Sanchez, C., Shelly, A., Sinha, B., Walters, D. N., West, A., Woollings, T., and Xavier, P. K.: The Met Office Global Coupled model 2.0 (GC2) configuration, Geosci. Model Dev., 8, 1509-1524, doi:10.5194/gmd-8-1509-2015, 2015.

Whitehead, J. D., Irwin, M., Allan, J. D., Good, N., and McFiggans, G.: A meta-analysis of particle water uptake reconciliation studies, Atmos. Chem. Phys., 14, 11833-11841, doi:10.5194/acp-14-11833-2014, 2014.

Woodward, S.: Modelling the atmospheric life cycle and radiative impact of mineral dust in the Hadley Centre climate model, J. Geophys. Res., 106, 18155–18166, 2001.

Woodward, S.: Mineral Dust in HadGEM2, Hadley Centre Technical Note 87, Met Office Hadley Centre for Climate Change, Exeter, United Kingdom, http://www.metoffice.gov.uk/archive/science/climatescience/ hctn87, 2011.

Wu, P., Christidis, N. and Stott, P.: Anthropogenic impact on Earth's hydrological cycle Nat. Clim. Change, 3, 807–10, doi:10.1038/nclimate1932, 2013.

Xia, L., Robock, A., Tilmes, S., and Neely III, R. R.: Stratospheric sulfate geoengineering enhances terrestrial gross primary productivity, Atmos. Chem. Phys. Discuss., 15, 25627-25645, doi:10.5194/acpd-15-25627-2015, 2015.

Zhang, Y., R. Fu, H. Yu, Y. Qian, R. Dickinson, M. A. F. Silva Dias, P. L. da Silva Dias, and K. Fernandes (2009), Impact of biomass burning aerosol on the monsoon circulation transition over Amazonia, Geophys. Res. Lett., 36, L10814, doi:10.1029/2009GL037180.

Aerosol scheme	Emitted particle properties			Scaling factors applied		
	Dg	σ	BC:OC	POM:OC conversion	Ageing growth factor	Global emission scaling
CLASSIC	0.20	1.3	0.093	n/a	1.62	1.6
GLOMAP-mode	0.15	1.59	Variable (GFED3.1)	1.4	n/a	2.0

Table 1. Biomass burning aerosol emissions: emitted particle properties and scaling factors applied.

Data source	Campaign / region	SSA	Å	$k_{ext,fm}$ (m^2/g)	g	References
models						
CLASSIC aged BBA	Global	0.91	2.3	5.0	0.58	Haywood et al. (2003)
GLOMAP-mode fine-mode	SAMBBA West (Rondonia)	0.87	2.0	4.8	0.63	
	SAMBBA East (Tocantins)	0.86	2.1	4.5	0.60	
	DABEX (West Africa)	0.85	2.0	4.6	0.61	
	SAFARI (S. Africa)	0.86	2.0	4.8	0.62	
Observations						
In-situ aircraft observations	SAMBBA West (Phase 1, Rondonia)[b]	0.88 +/- 0.05	1.9 +/- 0.3	3.6 +/- 0.06	[c]0.66 +/- 0.06 [d]0.59 +/- 0.05	Darbyshire et al. (in preparation, 2016), Brooke (2014)
	SAMBBA East (Tocantins)	0.79	2.1 +/- 0.2	n/a	0.57 +/- 0.05	Darbyshire et al. (in preparation, 2016).
	DABEX (West Africa)	0.81 +/- 0.05	1.7	5.8	0.63	Johnson et al. (2008)
	SAFARI-2000 (S. Africa)	0.88 +/- 0.04	n/a	4.3	0.58	Haywood et al. (2003)[e]

Table 2. Dry aerosol optical properties at 550nm from model and observations including Single Scattering Albedo (SSA), Ångström exponent (Å), fine-mode specific extinction coefficient ($k_{ext,fm}$), and asymmetry parameter (g). Error bounds are given to observed parameters, where available, to reflect uncertainty in the measurement.

[a] Assuming a representative mixture with 10 % fresh and 90 % aged BB aerosol.

[b] Phase 1 of SAMBBA was from 14 – 22 September 2012.

[c] Calculated from the nephelometer backscatter fraction based on Andrew et al. (2006).

[d] Derived from Mie calculations in Brooke (2014)

e Haywood et al. (2003) results for SSA reassessed in Johnson et al. (2008).

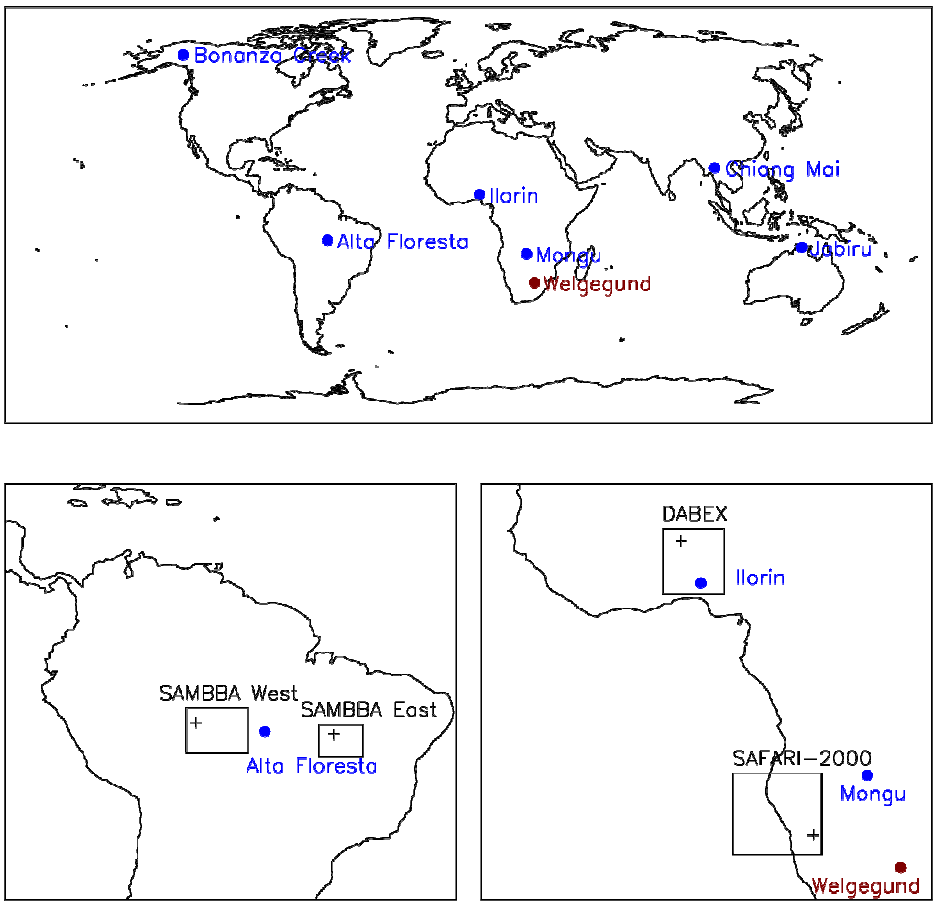

Figure 1. Maps showing the location of AERONET sites (blue), the Welgegund ground station, and the averaging boxes used corresponding to the flight regions from SAMBBA (West and East), DABEX and SAFARI-2000. Plus symbols indicate the locations of the main airbases used for the flights: Porto Velho for SAMBBA West, Palmas for SAMBBA East, Niamey for DABEX, and Windhoek for SAFARI-2000.

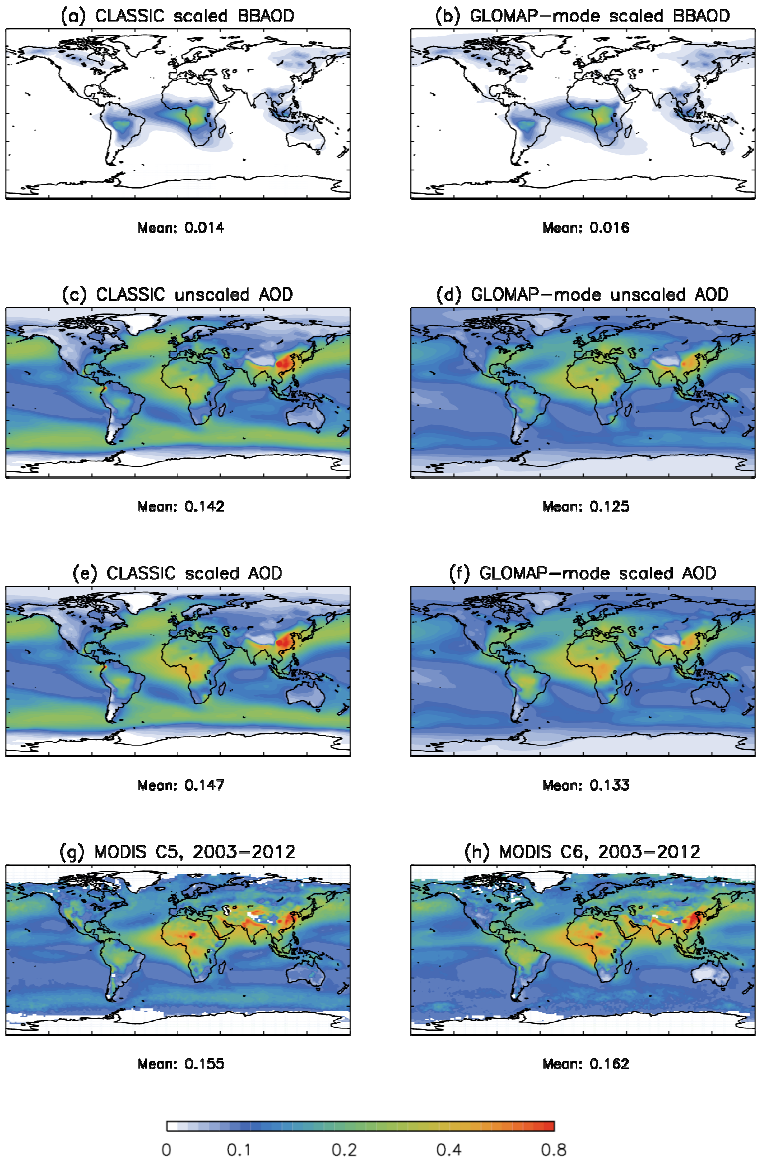

Figure 2. Decadal mean AOD at 550nm. Panels include: (a,b) BB AOD, the contribution of BBA emissions to the total AOD in the standard (scaled) simulations, (c,d) unscaled model AODs are from simulations that did not include scaling of BB aerosol emissions, (e,f) model AOD from the standard (scaled) simulations, (g,h) MODIS data from Aqua collections 5 and 6, averaged from 2003 – 2012. Model means from 2002 – 2011. Missing data values from MODIS are plotted as white.

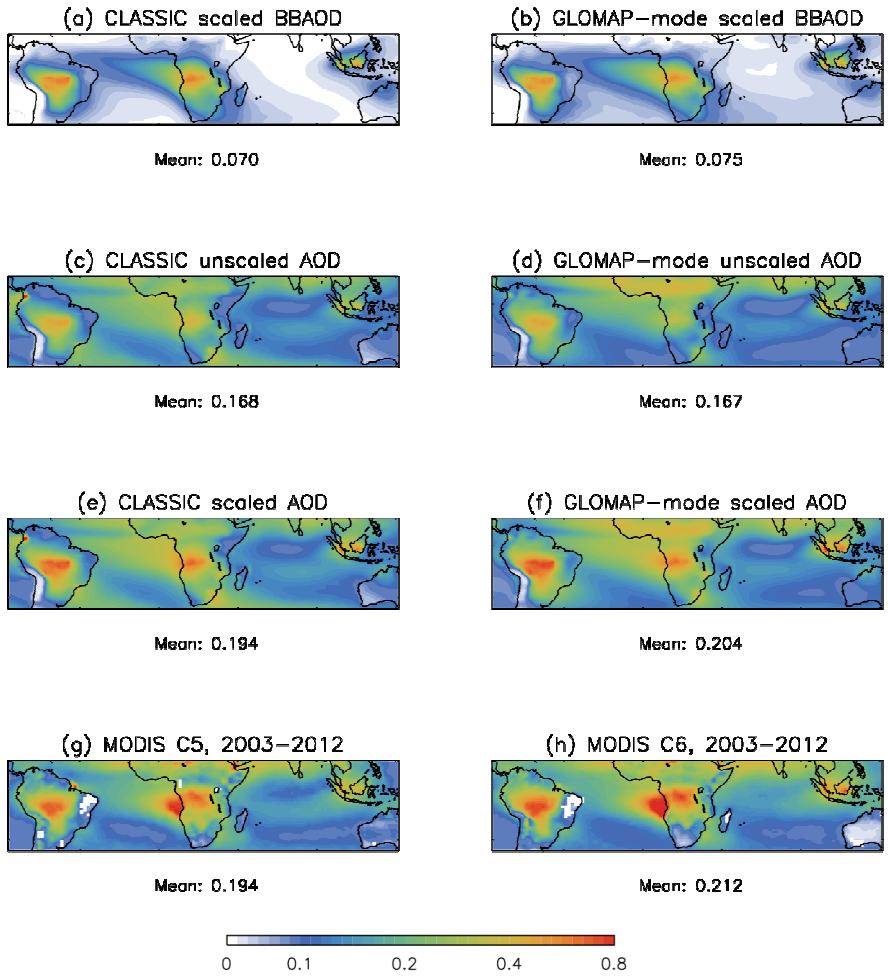

Figure 3. Same as Fig 2 but for the month of September.

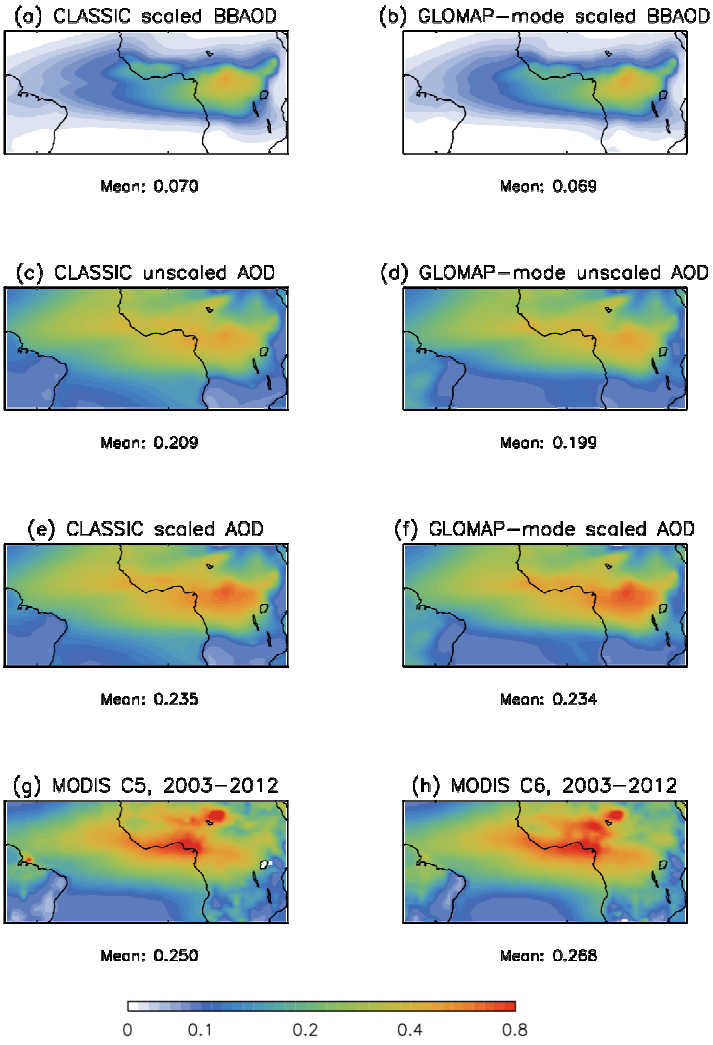

Figure 4. Same as Fig 2 but for the month of January.

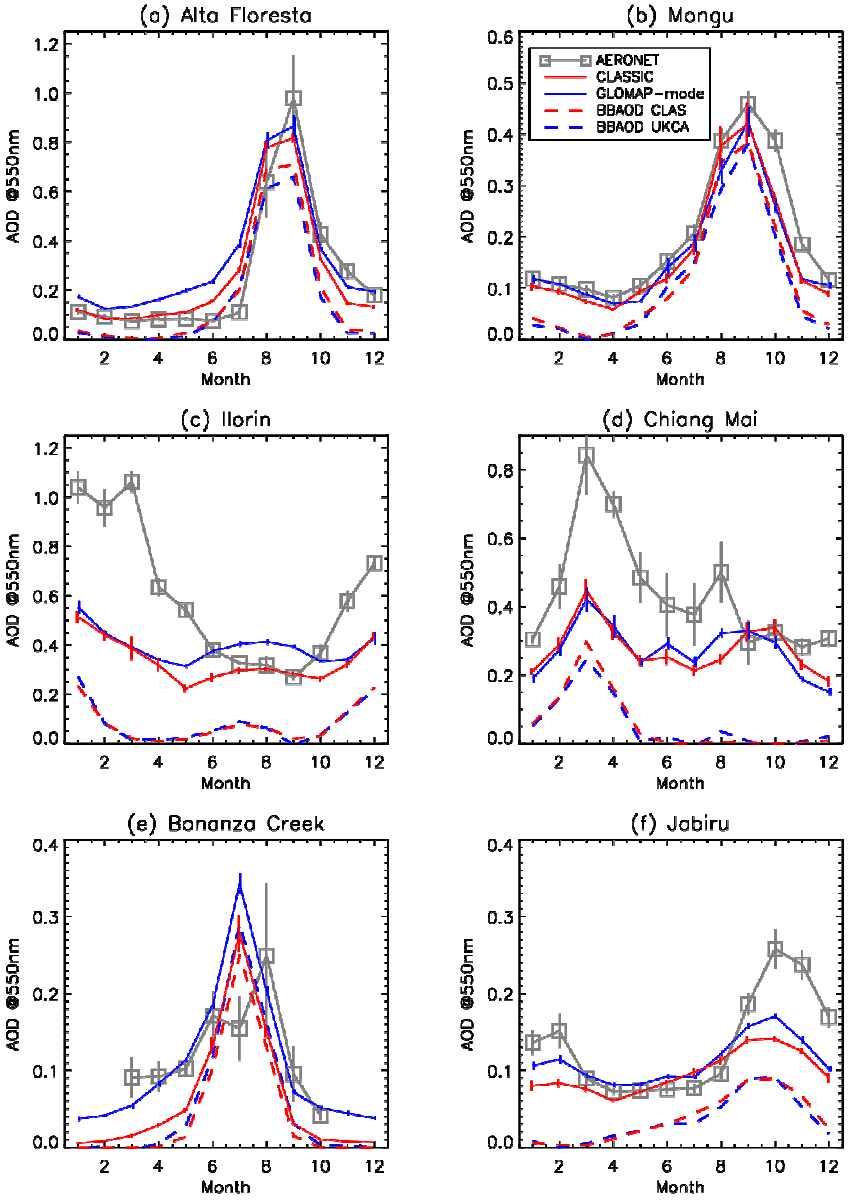

Figure 5. Monthly mean AOD at 550nm from six AERONET sites (grey squares), and the same locations from GLOMAP-mode (blue) and CLASSIC (red). The contribution to AOD from BBA is shown by dashed lines. Vertical lines show +/- 1 standard error.

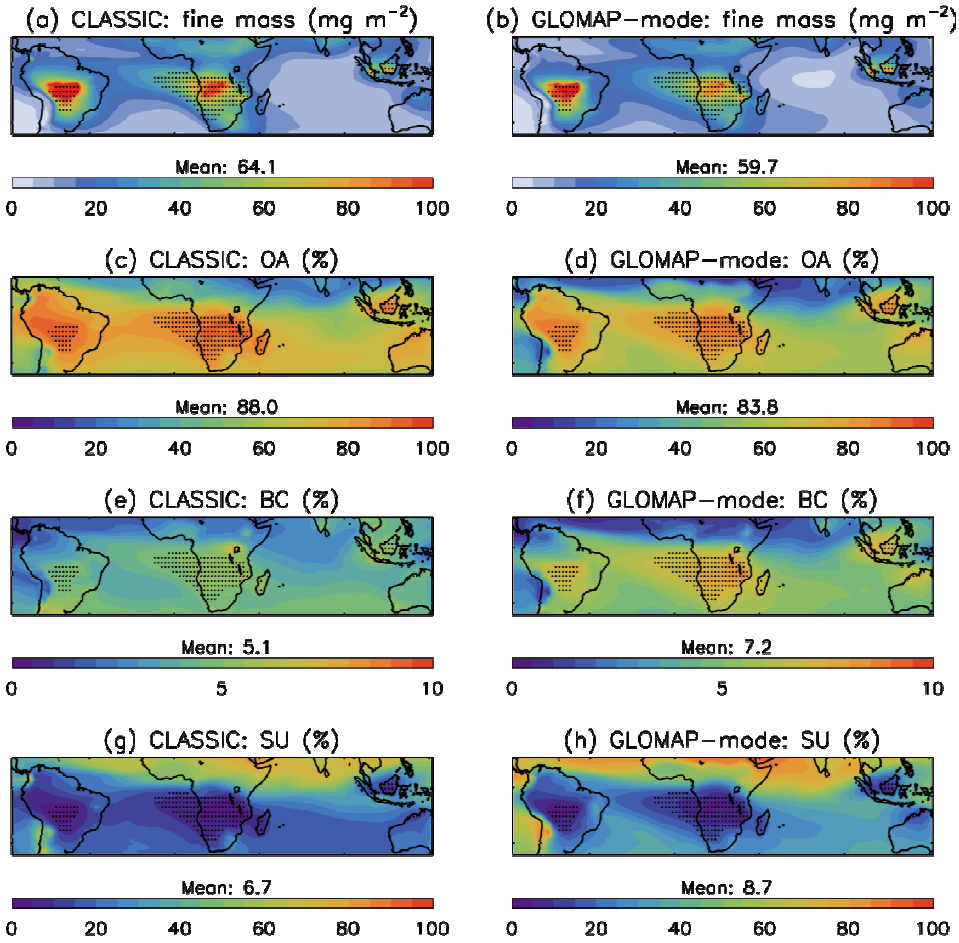

Figure 6. Modelled fine-mode aerosol composition from HadGEM3 for CLASSIC and GLOMAP-mode (including sulphate, BC and OA only). Plots show: (a, b) fine-mode mass burden (mg m^{-2}), (c, d) mass fraction of OA (%), (e, f) mass fraction of BC (%), (g, h) mass fraction of sulphate (%). Stipples indicate grid columns where more than 75 % of the fine-mode aerosol mass originates from biomass burning emissions (based on the speciation in the CLASSIC simulation). Mean values beneath each plot give the average from grid columns marked by these stipples.

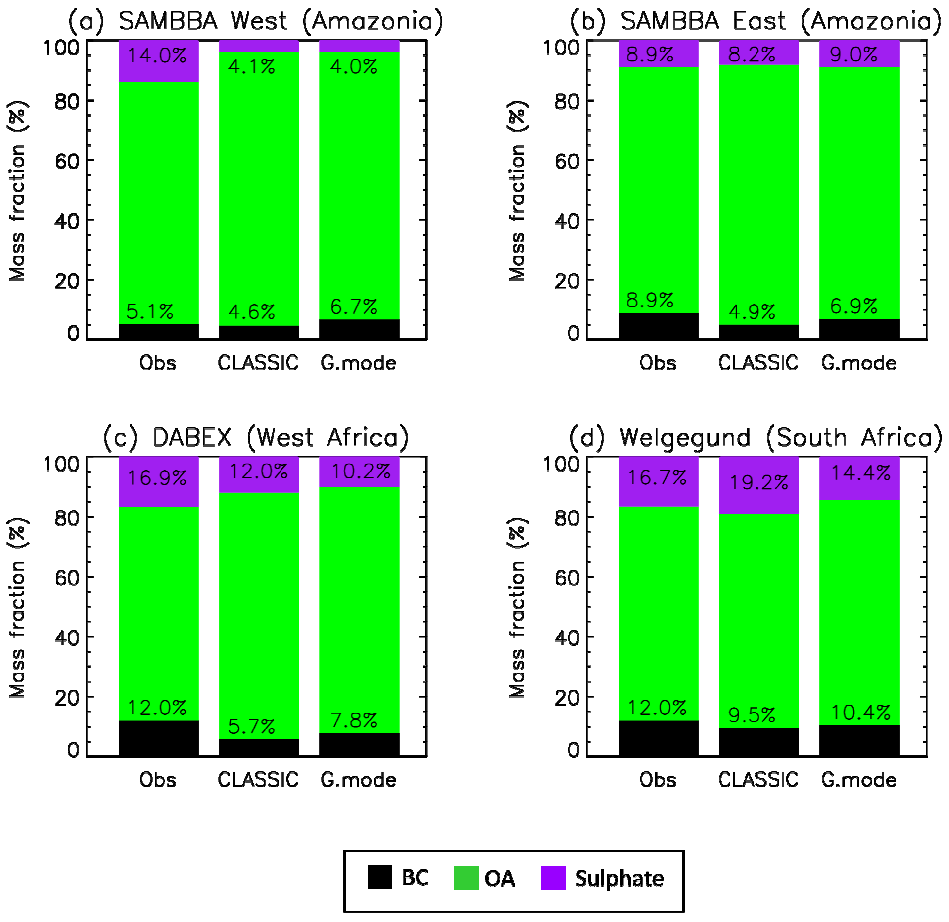

Figure 7. Mass fractions (%) of black carbon (black), organic aerosol (green), and sulphate (purple) (excluding other fine-mode aerosol components). Observed data are monthly averages from field campaigns including: SAMBBA (Amazonia, September 2012), DABEX (West Africa, Jan 2006), and the Welgegund site (South Africa, September 2010). Modelled data are long-term monthly mean values corresponding to the month and location of the observations. Welgegund model data is for aerosol composition at the surface (lowest model level), SAMBBA and DABEX model data is averaged over 0 – 5 km. The BC and sulphate mass fractions are labelled on each bar.

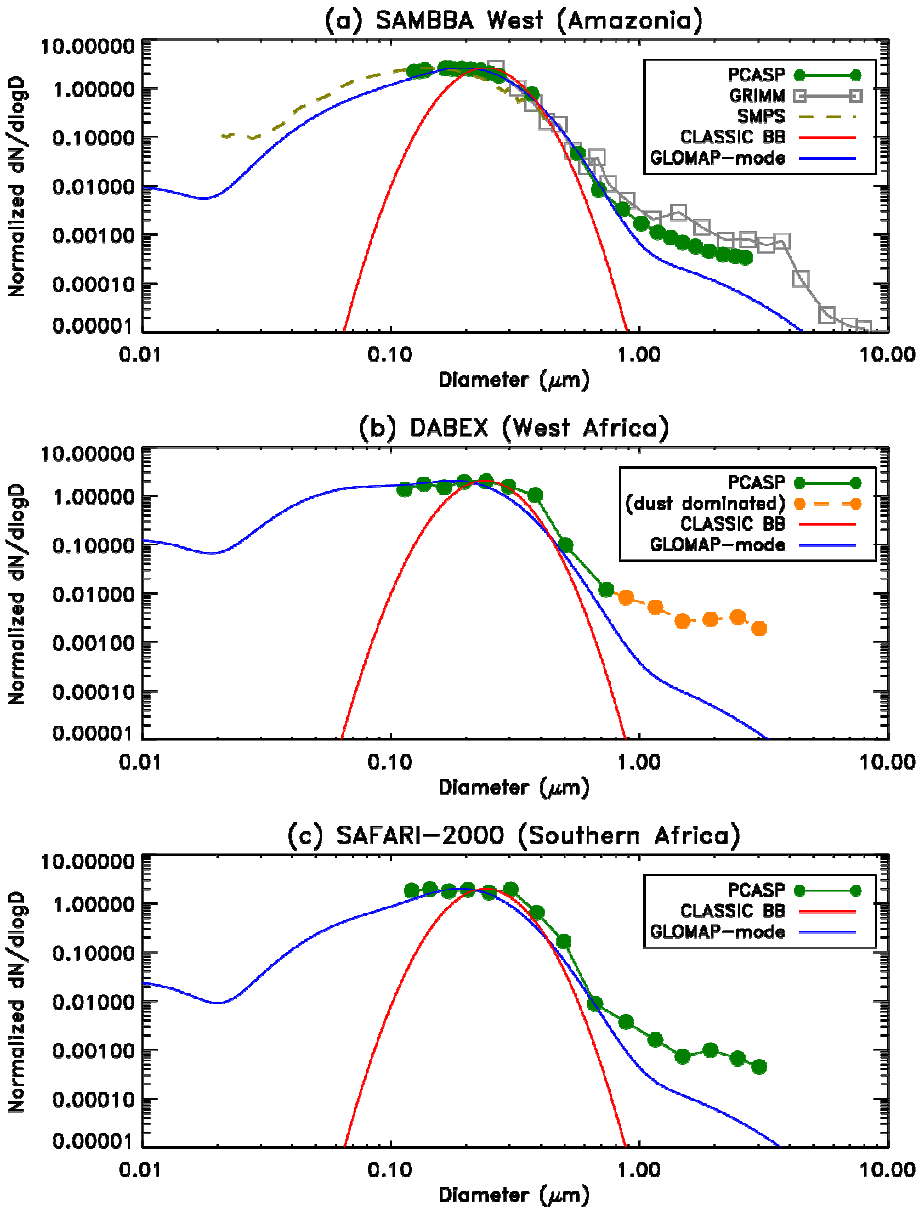

Figure 8. Aerosol number size distributions (dN/dlogD) versus particle diameter from aircraft observations (PCASP, GRIMM, SMPS) showing the mean distribution from three campaigns. CLASSIC curve is a representative mixture of 10 % fresh and 90 % aged BBA species, GLOMAP-mode is the complete size distribution over all 5 modes averaged over the flight regions in Fig. 1 and over 0 – 5 km.

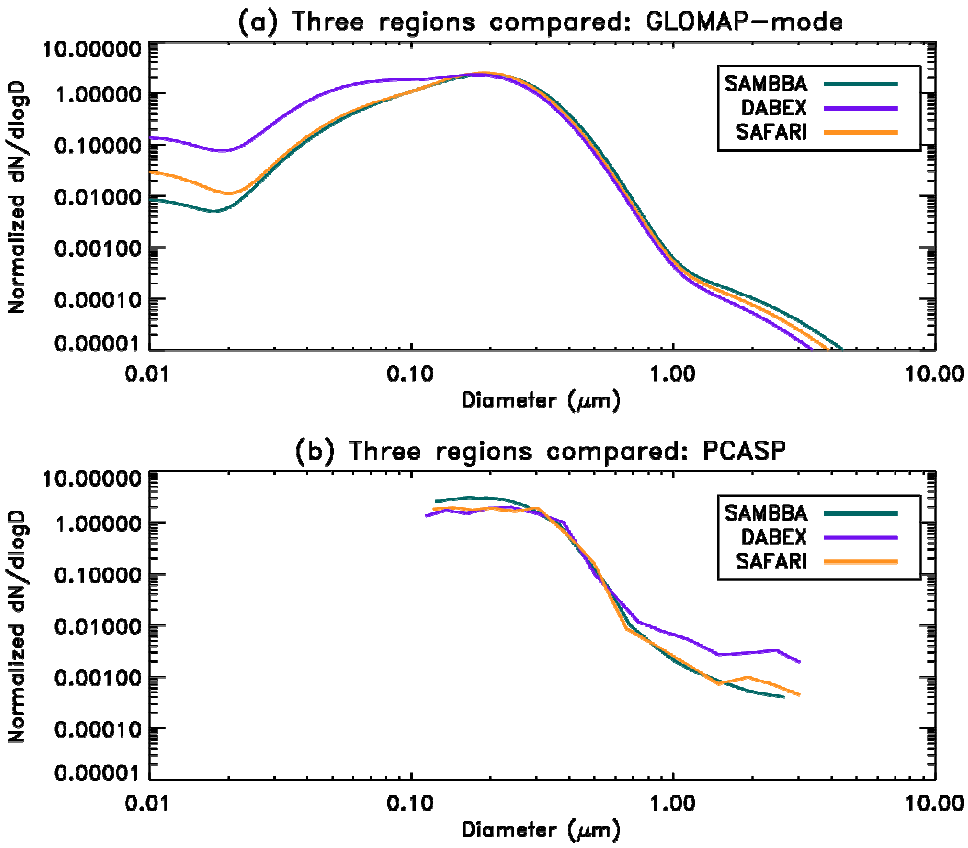

Figure 9. Same as Fig. 7 but showing only GLOMAP-mode curves and PCACP data.

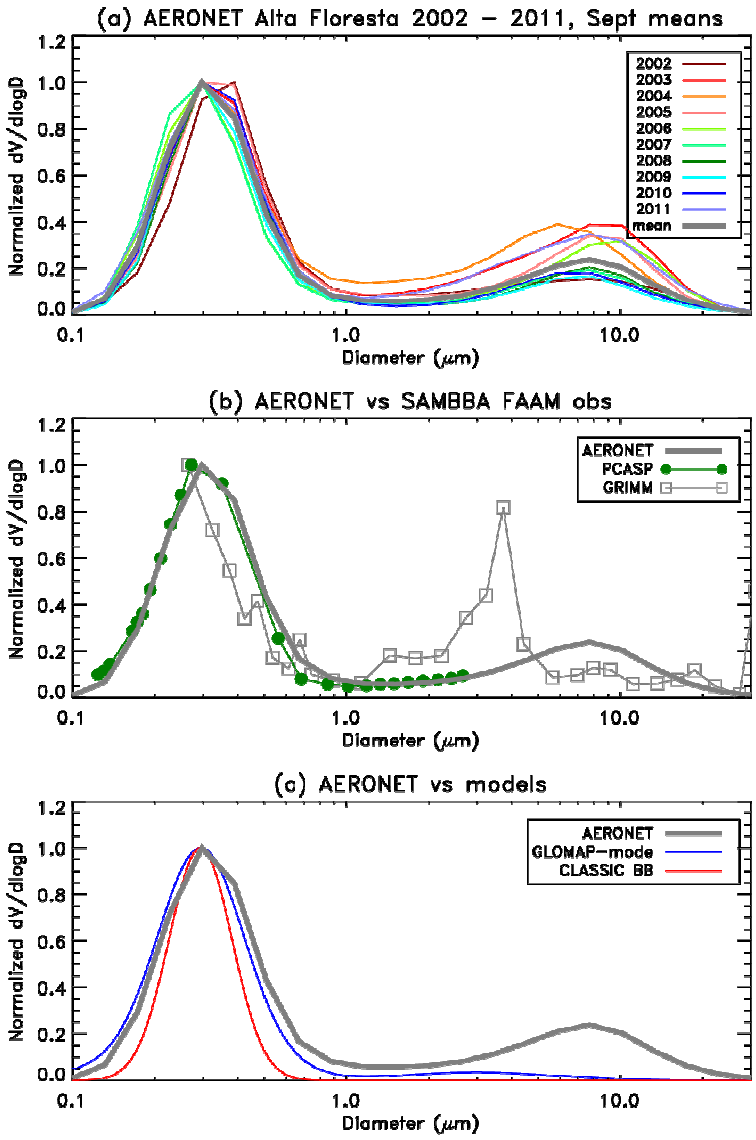

Figure 10. Aerosol volume size distributions (dV/dlogD $\mu m^3/ \mu m^2$) vs. particle diameter for (a) September means from AERONET Alta Floresta (Southern Amazonia) for 2002-2011 along with the long-term monthly mean from all years, (b) Comparison of AERONET 10-year September mean with FAAM averages from SAMBBA West region, normalized by peak concentration, (c) Comparison of AERONET 10-year September mean with HadGEM3 September monthly mean output, column-integrated mean over Alta Floresta for GLOMAP-mode (all active size modes) and CLASSIC (BB species only).

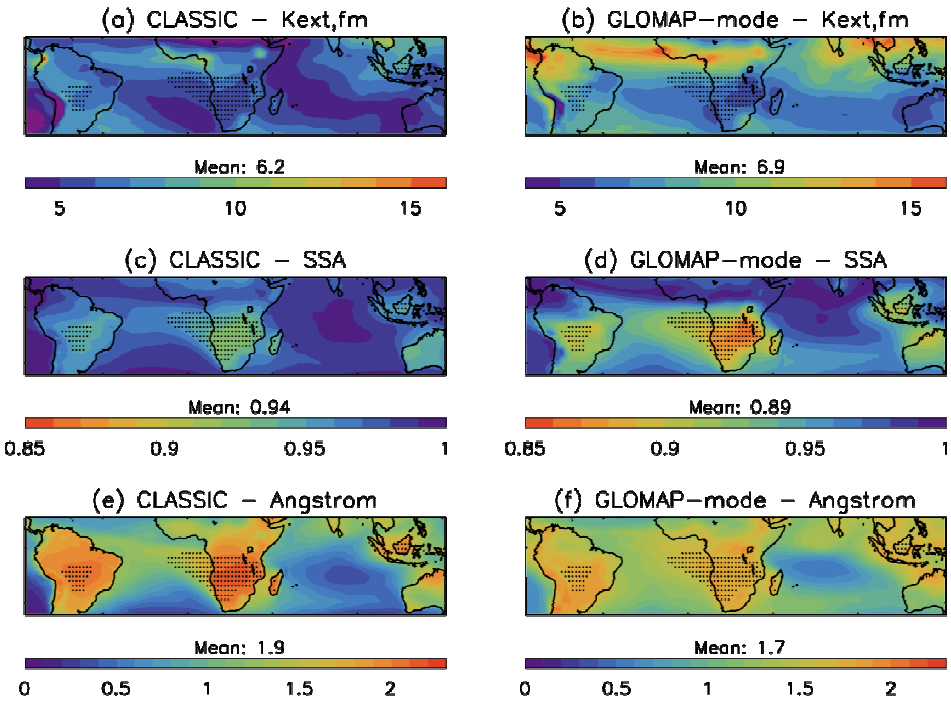

Figure 11. Column average moist aerosol optical properties from CLASSIC and GLOMAP-mode for September long-term monthly mean. Properties are the fine-mode specific extinction coefficient ($k_{ext,fm}$), Single Scattering Albedo (SSA) and Ångström exponent. Stipples indicate grid columns where more than 75 % of the fine-mode aerosol mass originates from biomass burning emissions (based on the speciation in the CLASSIC simulation). Mean values beneath each plot give the average from grid columns marked by these stipples.

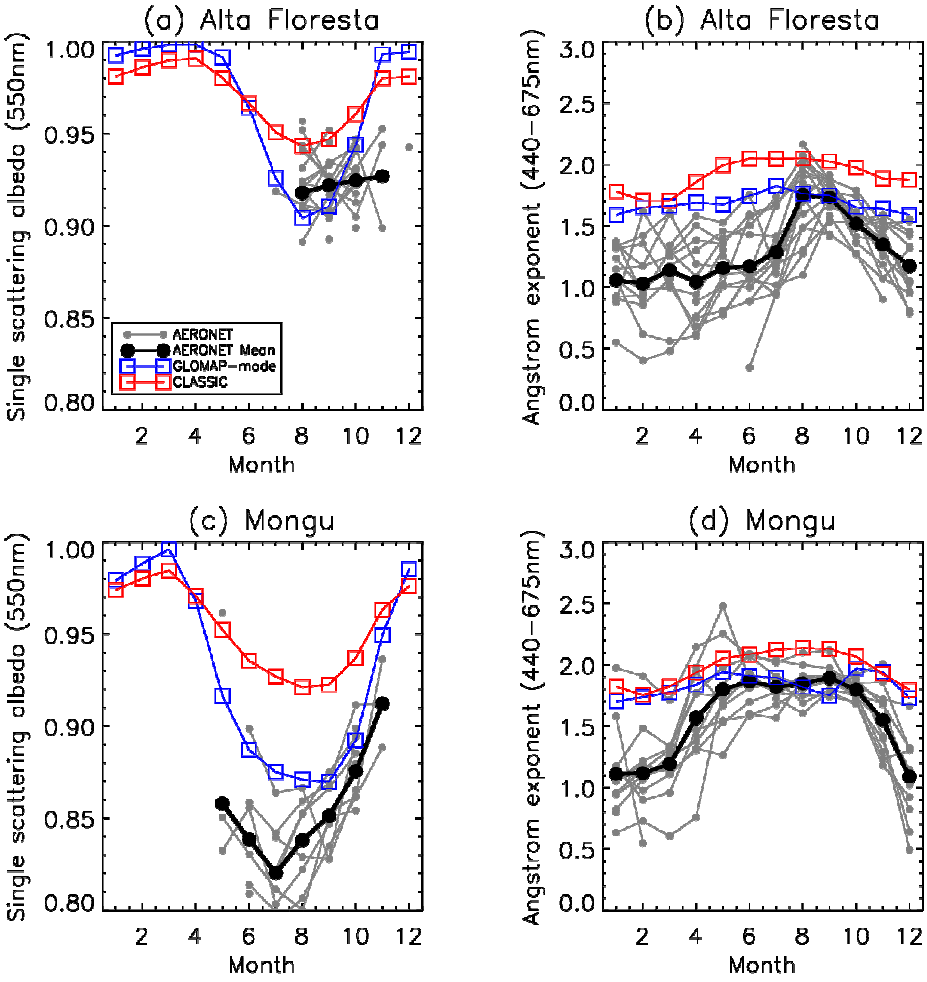

Figure 12. Seasonal cycle of moist aerosol optical properties (single scattering albedo and Ångström exponent). AERONET data from Alta Floresta (Southern Amazonia) and Mongu (Southern Africa) include all available monthly means (grey) and the long-term monthly mean (black) for months with good data coverage (see text). Co-located model data from GLOMAP-mode (red) and CLASSIC (blue) are shown taking the column average long-term monthly means.

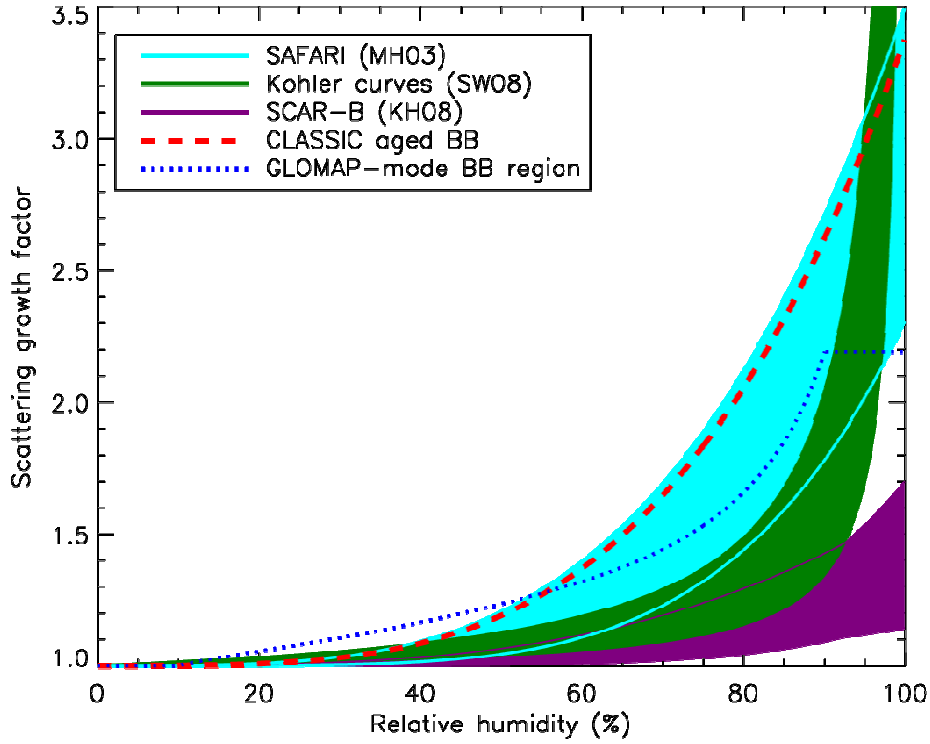

Figure 13. Hygroscopic growth curves showing the increase in aerosol scattering at 550nm with ambient relative humidity from a variety of observational sources and from the models. The curve for CLASSIC assumes a mixture of 10 % fresh and 90 % aged BBA. The curve for GLOMAP-mode is calculated based on the average composition from the four BB regions in Fig. 7. The solid filled areas show the range of growth factors estimated from each observation source (see text).

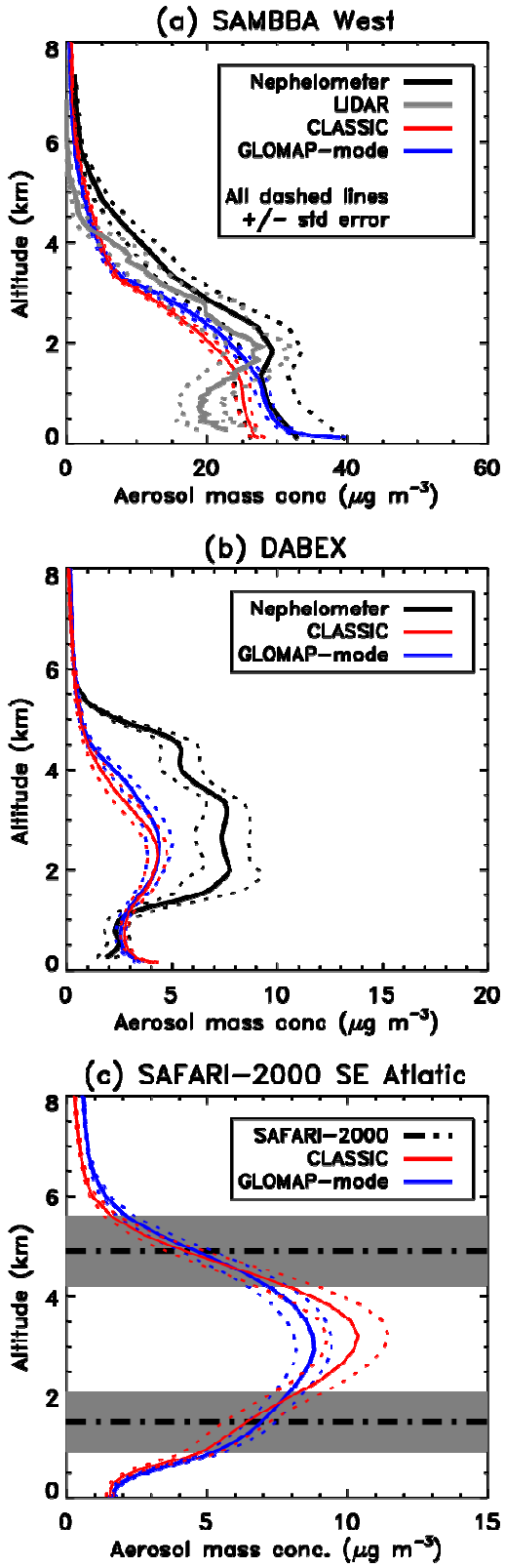
(a) SAMBBA West
Nephelometer
LIDAR
CLASSIC
GLOMAP–mode
All dashed lines
+/– std error
Altitude (km)
Aerosol mass conc (μg m⁻³)
(b) DABEX
Nephelometer
CLASSIC
GLOMAP–mode
Altitude (km)
Aerosol mass conc (μg m⁻³)
(c) SAFARI–2000 SE Atlatic
SAFARI–2000
CLASSIC
GLOMAP–mode
Altitude (km)
Aerosol mass conc. (μg m⁻³)

1

Figure 14. Vertical profiles of fine-mode aerosol mass concentration for the SAMBBA, DABEX and SAFARI-2000 airborne campaigns, including model averages for CLASSIC (red) and GLOMAP-mode (blue). Dashed lines show the mean +/- the standard error. Profiles of mass concentrations have been estimated from campaign-averaged nephelometer (black) and lidar (green) observations using the fine-mode specific scattering ($k_{sca,fm}$) and extinction coefficients ($k_{ext,fm}$), respectively, derived from the in-situ aircraft observations (see the second half of Table 2; $k_{sca,fm} = k_{ext,fm} * SSA$). The SAFARI-2000 observations indicate the average altitude of BBA layer base and top (black dot-dashed line) +/- the standard deviation (grey shading).